

# Extended Fourier analysis of signals

*Dr. Sc. Comp. Vilnis Liepiņš*

**Abstract**—This summary of the doctoral thesis [8] is created to emphasize the close connection of the proposed spectral analysis method and the Discrete Fourier Transform (DFT), the most extensively studied and frequently used approach in the history of signal processing. It is shown that in typical application case, where the uniform data readings are transformed to the same number of uniformly spaced frequencies, the results of the classical DFT and proposed approach coincide. Performance differences appear if the length of the DFT is selected greater than the length of the data. DFT resolves the problem of unknown data by padding readings with zeros up to DFT length, while the proposed Extended DFT (EDFT) deals with this situation in a different way, it uses Fourier integral transform as a target and optimizes the basis for transformation in the extended frequency set without imposing restrictions on the time domain. Consequently, Inverse DFT (IDFT), which is suitable for EDFT results, gives not only known readings but also the extrapolated data where classical DFT can only be returned zeros, and higher resolution is reached at frequencies where the data has been successfully extrapolated. EDFT has been shown to able to process data with missing readings or gaps inside or even nonuniformly sampled data. Therefore, EDFT significantly extends the usability of DFT based methods, where previously these approaches have been considered as not applicable [10-54]. EDFT finds a solution in an iterative way that requires repeated calculations to obtain an adaptive basis, and that makes numerical complexity much higher compared with DFT. This disadvantage was a serious problem in the 1990s, when the method was proposed. Fortunately, since then, computer power has increased so much that the use of EDFT can be a real alternative nowadays.

## 1 Introduction

A Fourier transform is a powerful tool for signal analysis and representation of a real or complex-valued function of time  $x(t)$  (hereinafter referred to as the signal) in the frequency domain

$$F(\omega) = \int_{-\infty}^{\infty} x(t)e^{-i\omega t} dt, \quad (1.1)$$

$$x(t) = \frac{1}{2\pi} \int_{-\infty}^{\infty} F(\omega)e^{i\omega t} d\omega. \quad (1.2)$$

The Fourier transforms orthogonality property provide a basis for the signal selective frequency analysis

$$\int_{-\infty}^{\infty} e^{-i\omega_0 t} e^{i\omega t} dt = 2\pi\delta(\omega - \omega_0), \quad (2)$$

where  $\omega, \omega_0$  are cyclic frequencies,  $i$  is an imaginary number such that  $i^2=-1$  and  $\delta(\omega-\omega_0)$  is the Dirac delta function. Unfortunately, the Fourier transforms calculation according to (1.1) requiring knowledge of the signal  $x(t)$  as well as performing of integration operation in the infinite time interval. Therefore, for practical evaluation of (1.1) numerically, the observation period and the interval of integration is always limited by some finite value  $\Theta$  and the signal is known in the time interval  $-\Theta/2 \leq t \leq \Theta/2$ . The same applies to the Fourier analysis of the signal sampled versions - nonuniformly sampled signal  $x(t_k)$  or uniformly sampled signal  $x(kT)$  for  $k=-\infty, \dots, -1, 0, 1, \dots, +\infty$ . Only a finite length sequence  $x(t_k)$  or  $x(kT)$ ,  $k=0, 1, 2, \dots, K-1$ , are subject of Fourier analysis, where  $K$  is a discrete sequence length,  $T$  is sampling period, and the signal observation period is equal to  $\Theta=t_{K-1}-t_0$  or  $\Theta=KT$ . To avoid aliasing and satisfy the Nyquist limit, uniform sampling of continuous time signals should be performed with the sampling period  $T \leq \pi/\Omega$ , where  $\Omega$  is the upper cyclic frequency of a signal  $x(t)$ . Although nonuniform sampling has no such a strict limitation on the mean sampling period  $T_s=\Theta/K$ , in the subsequent analysis we suppose that both sequences,  $x(t_k)$  and  $x(kT)$ , are derived from a band-limited in  $\Omega$  signal  $x(t)$ . Let's write the basic expressions of classical and extended Fourier analysis of continuous time signal  $x(t)$  and its sampled versions  $x(t_k)$  and  $x(kT)$ .

## 2 Problem formulation

“The formulation of a problem is often more essential than its solution which may be merely a matter of mathematical or experimental skill. To raise new questions, new possibilities, to regard old problems from a new angle requires creative imagination and marks real advances in science.”

*Albert Einstein and Léopold Infeld, Evolution of Physics, 1938.*

### 2.1 Basic expressions of classical Fourier analysis

The classical Fourier analysis dealing with the following finite time Fourier transforms

$$F_{\Theta}(\omega) = \int_{-\Theta/2}^{\Theta/2} x(t)e^{-i\omega t} dt, \quad (3.1a)$$

$$F_{\Theta}(\omega) = \sum_{k=0}^{K-1} x(t_k)e^{-i\omega t_k}, \quad (3.1b)$$

$$F_{\Theta}(\omega) = \sum_{k=0}^{K-1} x(kT)e^{-i\omega kT}, \quad (3.1c)$$

$$x_{\Theta}(t) = \frac{1}{2\pi} \int_{-\Omega}^{\Omega} F_{\Theta}(\omega)e^{i\omega t} d\omega, \quad (3.2)$$

where (3.2) is the inverse Fourier transform obtained from (1.2) for a band-limited in  $\Omega$  signal. Transforms (3.1b) and (3.1c) are known as Discrete Time Fourier Transforms (DTFT) of the nonuniformly and uniformly sampled signals. The reconstructed signal  $x_{\Theta}(t)$  outside the observation period  $\Theta$  vanishes quickly reaching values close to zeros. The signal amplitude spectrum is the Fourier transform (3.1) divided by the observation period

$$S_{\Theta}(\omega) = \frac{1}{\Theta} F_{\Theta}(\omega). \quad (4)$$

The frequency resolution of the classical Fourier analysis is inversely proportional to the observation period  $\Theta$ , thus, the longer interval of signal analysis, the higher resolution is achieved. Obviously, one can get the formula (3.1a) by truncation of infinite integration limits in (1.1) and the DTFT (3.1b) and (3.1c) in a result of replacement of infinite sums by finite ones. This means, the classical Fourier analysis supposed that the signal outside  $\Theta$  is zero. In other words, the Fourier transform calculation by formulas (3.1) is well justified if applied to time-limited within  $\Theta$  signals. On the other hand, a band-limited in  $\Omega$  signal cannot be also time-limited and obviously have nonzero values outside  $\Theta$ . Generally, the Fourier analysis results obtained by using the exponential basis tend to the Fourier transform when  $\Theta \rightarrow \infty$ , while at any finite  $\Theta$  another transform basis may exist that provides a more accurate estimate of (1.1).

### 2.2 Basic expressions of extended Fourier analysis

The idea of extended Fourier analysis is finding the transform basis, applicable to a band-limited signals registered in the finite time interval  $\Theta$  and providing the results as close as possible in terms of the  $L^2$ -norm (or the Euclidean norm) to the Fourier transform (1.1) defined in the infinite time interval. The formulas for proposed extended Fourier analysis could be written as

$$F_{\alpha}(\omega) = \int_{-\Theta/2}^{\Theta/2} x(t)\alpha(\omega, t) dt, \quad (5.1a)$$

$$F_{\alpha}(\omega) = \sum_{k=0}^{K-1} x(t_k)\alpha(\omega, t_k), \quad (5.1b)$$

$$F_\alpha(\omega) = \sum_{k=0}^{K-1} x(kT)\alpha(\omega, kT), \quad (5.1c)$$

$$x_\alpha(t) = \frac{1}{2\pi} \int_{-\Omega}^{\Omega} F_\alpha(\omega) e^{i\omega t} d\omega, \quad (5.2)$$

where in general case the transform basis  $\alpha(\omega, t)$ ,  $\alpha(\omega, t_k)$  and  $\alpha(\omega, kT)$  are not equal to the classical ones (3.1). Note that the inverse Fourier transform (5.2) still preserves the exponential basis and Parseval-Planchered equality  $\int_{-\infty}^{\infty} |x_\alpha(t)|^2 dt = \frac{1}{2\pi} \int_{-\Omega}^{\Omega} |F_\alpha(\omega)|^2 d\omega$  holds for it.

To ensure that the results of transforms (5.1) are close to the result of the Fourier transform (1.1) for signal  $x(t)$ , the following minimum least squares expression will be constructed and solved

$$|F(\omega) - F_\alpha(\omega)|^2 \rightarrow \min. \quad (6)$$

Unfortunately, as already stated above, the calculation of  $F(\omega)$  cannot be performed directly for a band-limited signal. So, to compose (6) we need to find an adequate substitution. Let's recall that a complex exponent at cyclic frequency  $\omega_0$  and with a complex amplitude  $S(\omega_0)$  is defined in the infinite time interval as

$$x(\omega_0, t) = S(\omega_0) e^{i\omega_0 t}, \quad -\infty < t < \infty. \quad (7)$$

The Fourier transform of a signal (7) can be expressed by the Dirac delta function (2)

$$\int_{-\infty}^{\infty} x(\omega_0, t) e^{-i\omega t} dt = 2\pi S(\omega_0) \delta(\omega - \omega_0). \quad (8)$$

Now, we will use (7) as a signal model with known amplitude spectrum  $S(\omega_0)$  for frequencies in the range  $-\Omega \leq \omega_0 \leq \Omega$  and in the expression (6) substitute  $F(\omega)$  by the Fourier transform of the signal model (8) and signals  $x(t)$ ,  $x(t_k)$  and  $x(kT)$  in (5.1) by signal models (7), respectively. Finally, the integral least squares error estimators for all three signal cases take the form

$$\Delta = \int_{-\Omega}^{\Omega} \left| 2\pi S(\omega_0) \delta(\omega - \omega_0) - \int_{-\Theta/2}^{\Theta/2} S(\omega_0) e^{i\omega_0 t} \alpha(\omega, t) dt \right|^2 d\omega_0, \quad (9a)$$

$$\Delta = \int_{-\Omega}^{\Omega} \left| 2\pi S(\omega_0) \delta(\omega - \omega_0) - \sum_{k=0}^{K-1} S(\omega_0) e^{i\omega_0 t_k} \alpha(\omega, t_k) \right|^2 d\omega_0, \quad (9b)$$

$$\Delta = \int_{-\Omega}^{\Omega} \left| 2\pi S(\omega_0) \delta(\omega - \omega_0) - \sum_{k=0}^{K-1} S(\omega_0) e^{i\omega_0 kT} \alpha(\omega, kT) \right|^2 d\omega_0. \quad (9c)$$

Solutions (9) for a definite signal model (7) provide the basis  $\alpha(\omega, t)$ ,  $\alpha(\omega, t_k)$  and  $\alpha(\omega, kT)$  for the extended Fourier transforms (5.1). To control how close amplitudes  $S(\omega_0)$  of the selected signal model are to the amplitude spectrum of the signals  $x(t)$ ,  $x(t_k)$  and  $x(kT)$ , we will find formulas for estimating the amplitude spectrum  $S_\alpha(\omega)$  in the basis  $\alpha(\omega, t)$ ,  $\alpha(\omega, t_k)$  and  $\alpha(\omega, kT)$ .

Formula (8) reveals the relationship between the Fourier transform of signal model and its amplitude spectrum, from where  $S(\omega_0)$  could be expressed as the Fourier transform of signal model divided by  $2\pi\delta(\omega-\omega_0)$ . Taking (8) into account,  $S_\alpha(\omega)$  is calculated as transforms (5.1) divided by the estimate  $2\pi\delta(\omega-\omega_0)$  in the extended Fourier basis, which is determined from (9) in the case of  $\Delta=0$  and  $\omega_0=\omega$ ,

$$S_\alpha(\omega) = \frac{\int_{-\Theta/2}^{\Theta/2} x(t) \alpha(\omega, t) dt}{\int_{-\Theta/2}^{\Theta/2} e^{i\omega t} \alpha(\omega, t) dt}, \quad (10a)$$

$$S_\alpha(\omega) = \frac{\sum_{k=0}^{K-1} x(t_k) \alpha(\omega, t_k)}{\sum_{k=0}^{K-1} e^{i\omega t_k} \alpha(\omega, t_k)}, \quad (10b)$$

$$S_{\alpha}(\omega) = \frac{\sum_{k=0}^{K-1} x(kT) \alpha(\omega, kT)}{\sum_{k=0}^{K-1} e^{i\omega kT} \alpha(\omega, kT)}, \quad (10c)$$

and show that the amplitude spectrum at frequency  $\omega$  is estimated as ratio of the signal extended Fourier transform to the transform of exponent with a unit amplitude in the same basis. This is also true for the classical Fourier analysis, for example, after substituting the exponential basis  $\alpha(\omega, t) = e^{-i\omega t}$  in (10a), its denominator becomes equal to  $\Theta$  as in formula (4) for the classical Fourier transform.

The denominator in formulas (10) is inversely proportional to the frequency resolution of the extended Fourier transform.

Before finding the extended basis functions for arbitrary  $S(\omega_0)$ , it is reasonable to consider a simple signal model having a rectangular form,  $S(\omega_0)=1$  for  $-\Omega \leq \omega_0 \leq \Omega$  and zeros outside. Then the estimators (9) reduce to

$$\Delta = \int_{-\Omega}^{\Omega} \left| 2\pi\delta(\omega - \omega_0) - \int_{-\Theta/2}^{\Theta/2} e^{i\omega_0 t} \alpha(\omega, t) dt \right|^2 d\omega_0, \quad (11a)$$

$$\Delta = \int_{-\Omega}^{\Omega} \left| 2\pi\delta(\omega - \omega_0) - \sum_{k=0}^{K-1} e^{i\omega_0 t_k} \alpha(\omega, t_k) \right|^2 d\omega_0, \quad (11b)$$

$$\Delta = \int_{-\Omega}^{\Omega} \left| 2\pi\delta(\omega - \omega_0) - \sum_{k=0}^{K-1} e^{i\omega_0 kT} \alpha(\omega, kT) \right|^2 d\omega_0. \quad (11c)$$

The solution (11) allows us to establish a relationship between the classical and extended Fourier transforms.

### 3 Problem solution

In this section the integral least squares error estimators (9) and (11) are solved and subsequent analysis of the obtained results is carried out in order to find only those solutions that can lead to practically implementable algorithms.

#### 3.1 Extended Fourier transform of continuous time signals

The solution of (11a) for continuous time signal  $x(t)$  is found as a partial derivation  $\frac{\partial \Delta}{\partial \alpha(\omega, \tau)} = 0$ ,  $-\frac{\Theta}{2} \leq \tau \leq \frac{\Theta}{2}$ , and leads to the linear integral equation

$$\int_{-\Theta/2}^{\Theta/2} \frac{\sin(\Omega(t - \tau))}{\pi(t - \tau)} \alpha(\omega, t) dt = e^{-i\omega\tau}. \quad (12)$$

Step by step solution of (12) is given in [4]. Finally, the basis  $\alpha(\omega, t)$  are obtained by applying a specific function system - a prolate spheroidal wave functions [1]  $\psi_k(t)$ ,  $k=0,1,2,\dots$ , and are written as series expansion

$$\alpha(\omega, t) = \sum_{k=0}^{\infty} \frac{B_k(\omega)}{\lambda_k} \psi_k(t). \quad (13)$$

The extended Fourier Transform of continuous time signal  $x(t)$  are given by

$$F_{\alpha}(\omega) = \sum_{k=0}^{\infty} B_k(\omega) a_k, \quad -\Omega \leq \omega \leq \Omega, \quad (14.1)$$

$$x_{\alpha}(t) = \sum_{k=0}^{\infty} \psi_k(t) a_k, \quad -\infty < t < \infty, \quad (14.2)$$

$$S_\alpha(\omega) = \frac{\sum_{k=0}^{\infty} B_k(\omega) a_k}{\sum_{k=0}^{\infty} |B_k(\omega)|^2}, \quad (14.3)$$

where  $a_k = \frac{1}{\lambda_k} \int_{-\Theta/2}^{\Theta/2} x(\tau) \psi_k(\tau) d\tau$ ,  $\lambda_k = \int_{-\Theta/2}^{\Theta/2} \psi_k^2(t) dt$ ,  $B_k(\omega) = \sqrt{\frac{\pi\Theta}{\lambda_k\Omega}} \psi_k(\omega \frac{\Theta}{2\Omega}) (-i)^k$  and the Parseval-Plancherel equality gives  $\int_{-\infty}^{\infty} |x_\alpha(t)|^2 dt = \frac{1}{2\pi} \int_{-\Omega}^{\Omega} |F_\alpha(\omega)|^2 d\omega = \sum_{k=0}^{\infty} |a_k|^2$ .

The extended Fourier transform in accordance with (14.1) requesting a calculation of infinite sums, this means, an infinite quantity of mathematical operations, therefore it's impossible for real world applications. Theoretically, the value of denominator  $\sum_{k=0}^K |B_k(\omega)|^2$  in the amplitude spectrum formula (14.3) tends to infinite as  $K \rightarrow \infty$  and the extended Fourier transform (14.1) provides super-resolution - an ability to determine the Fourier transform for sums of sinusoids or complex exponents, if their frequencies differ by an arbitrarily small finite value.

## 3.2 Extended Discrete Time Fourier Transform

In this subsection the minimum least squares error estimators (9b,c) and (11b,c) are solved and the extended Fourier transforms for uniformly and nonuniformly sampled complex-valued signals are obtained. The proposed approaches have been developed in articles [5, 6], where the derivations for real-valued discrete signals are given.

The following notations are used in the matrix equations: superscripts  $\mathbf{X}^{-1}$ ,  $\mathbf{X}^T$ ,  $\mathbf{X}^*$  and  $\mathbf{X}^H$  denote inverse, transpose, complex conjugate and complex conjugate (Hermitian) transpose of the matrix  $\mathbf{X}$ ;  $/$  represents element-by-element division of two matrices with the same size;  $sum(\mathbf{X})$  means addition of all matrix  $\mathbf{X}$  elements and the  $diag(\mathbf{X})$  forms the row vector by extracting the main diagonal elements from quadratic matrix  $\mathbf{X}$  or it puts the elements of vector  $\mathbf{X}$  on the main diagonal to form a diagonal matrix.

### 3.2.1 Particular solution for discrete time signals

The solutions of (11b,c) can be obtained similarly to (11a), as partial derivatives of  $\frac{\partial \Delta}{\partial \alpha(\omega, t_l)} = 0$  and  $\frac{\partial \Delta}{\partial \alpha(\omega, lT)} = 0$  for  $l=0,1,2,\dots,K-1$ , and leads to the systems of linear equations

$$\sum_{k=0}^{K-1} \frac{\sin(\Omega(t_k - t_l))}{\pi(t_k - t_l)} \alpha(\omega, t_k) = e^{-i\omega t_l}, \quad (15a)$$

$$\sum_{k=0}^{K-1} \frac{\sin(\Omega(k - l)T)}{\pi(k - l)T} \alpha(\omega, kT) = e^{-i\omega lT}. \quad (15b)$$

The solution of (15) in the matrix form is expressed as

$$\mathbf{A}_\omega = \mathbf{R}^{-1} \mathbf{E}_\omega, \quad (16)$$

where  $\mathbf{A}_\omega (K \times 1)$  and  $\mathbf{E}_\omega (K \times 1)$  are the extended Fourier and the exponential basis.

The formulas of Extended Discrete Time Fourier Transform (EDTFT) for signal model  $S(\omega_0)=1$ ,  $-\Omega \leq \omega_0 \leq \Omega$ , are derived by substituting of transformation basis (16) into expressions (5) and (10)

$$F_\alpha(\omega) = \mathbf{x} \mathbf{R}^{-1} \mathbf{E}_\omega, \quad -\Omega \leq \omega \leq \Omega, \quad (17.1)$$

$$x_\alpha(t) = \mathbf{x} \mathbf{R}^{-1} \mathbf{E}_t, \quad -\infty < t < \infty, \quad (17.2)$$

$$S_\alpha(\omega) = \frac{\mathbf{x} \mathbf{R}^{-1} \mathbf{E}_\omega}{\mathbf{E}_\omega^H \mathbf{R}^{-1} \mathbf{E}_\omega}. \quad (17.3)$$

The matrices for nonuniformly sampled signal  $x(t_k)$  are composed as follows

$$\mathbf{x} (1 \times K): x(t_k), \mathbf{E}_\omega (K \times 1): e^{-i\omega t_l}, \mathbf{R} (K \times K): r_{l,k} = \frac{\sin(\Omega(t_k - t_l))}{\pi(t_k - t_l)}, \mathbf{E}_t (K \times 1): e_l = \frac{\sin(\Omega(t - t_l))}{\pi(t - t_l)}.$$

Uniformly sampled sequence  $x(kT)$  could be considered as a special case of nonuniform sampling at time moments  $t_k = kT$ ,  $k=0,1,2,\dots,K-1$ , then the matrices in (16, 17) are formed as

$$\mathbf{x}(1 \times K): x(kT), \mathbf{E}_\omega (K \times 1): e^{-i\omega lT}, \mathbf{R} (K \times K): r_{l,k} = \frac{\sin(\Omega(k-l)T)}{\pi(k-l)T}, \mathbf{E}_l (K \times 1): e_l = \frac{\sin(\Omega(t-lT))}{\pi(t-lT)}.$$

If sampling of signal  $x(kT)$  is done with Nyquist rate,  $T=\pi/\Omega$ , the matrix  $\mathbf{R}$  becomes a unit matrix  $\mathbf{I}$  and the formula (17.1) coincide with classical DTFT (3.1c), but the formula (17.3) reduces to the well-known relationship between discrete signal Fourier transform and its amplitude spectrum

$$F_\alpha(\omega) = F_\Theta(\omega) = \mathbf{x}\mathbf{E}_\omega, \quad (18.1)$$

$$S_\alpha(\omega) = \frac{1}{K} \mathbf{x}\mathbf{E}_\omega. \quad (18.2)$$

Whereas for nonuniformly sampled signal  $x(t_k)$  the matrix  $\mathbf{R} \neq \mathbf{I}$ , even if mean sampling period  $T_s = \pi/\Omega$  and formulas (17) give the results that are close to uniform case and superior to those obtained by the classical nonuniform DTFT (3.1b). The resolution by frequency in both sampling cases equals to  $1/KT$ , which is a normal frequency resolution. While for oversampled signals,  $T$  (or  $T_s$ )  $< \pi/\Omega$ , the EDTFT approach can provide a high frequency resolution and improved spectral estimation quality. Unfortunately, an achievement of such results is limited by finite precision in the mathematical calculations and by restrictions on frequency range in the process of signal sampling. The theoretical value of the denominator in (17.3)  $\mathbf{E}_\omega^H \mathbf{R}^{-1} \mathbf{E}_\omega = K$  and the frequency resolution should increase proportionally to the number of samples in the signal observation period  $\Theta$ . In the border-case, if the number of samples within  $\Theta$  increases to infinity,  $K \rightarrow \infty$ , and the discrete time signal tends to the continuous time signal  $x(t)$ , the EDTFT (17.1) gives the same result as (14.1).

### 3.2.2 Generalized solution for discrete time signals

Now, we will consider the solution of the minimum least squares error estimators (9b,c) for arbitrary selected signal model  $S(\omega_0)$ . The derivation formulas for both estimators are like the ones given in the previous section. For example, a partial derivation of (9b) by the basis,  $\frac{\partial \Delta}{\partial \alpha(\omega, t_l)} = 0$  for  $l=0,1,2,\dots,K-1$ , provides the least squares solution

$$\int_{-\Omega}^{\Omega} \left( 2\pi S(\omega_0) \delta(\omega - \omega_0) - \sum_{k=0}^{K-1} S(\omega_0) e^{i\omega_0 t_k} \alpha(\omega, t_k) \right) S^*(\omega_0) e^{-i\omega_0 t_l} d\omega_0 = 0, \quad (19)$$

Equation (19) can be rewritten as

$$\sum_{k=0}^{K-1} \left( \int_{-\Omega}^{\Omega} |S(\omega_0)|^2 e^{i\omega_0(t_k - t_l)} d\omega_0 \right) \alpha(\omega, t_k) = 2\pi \int_{-\Omega}^{\Omega} |S(\omega_0)|^2 e^{-i\omega_0 t_l} \delta(\omega - \omega_0) d\omega_0. \quad (20)$$

The filtering feature of the Dirac delta function  $\int_{-\infty}^{\infty} f(x) \delta(x - x_0) dx = f(x_0)$  applied to the right part of (20) gives the final form of the system of linear equations for  $l=0,1,2,\dots,K-1$ ,

$$\sum_{k=0}^{K-1} \left( \frac{1}{2\pi} \int_{-\Omega}^{\Omega} |S(\omega_0)|^2 e^{i\omega_0(t_k - t_l)} d\omega_0 \right) \alpha(\omega, t_k) = |S(\omega)|^2 e^{-i\omega t_l}, \quad (21a)$$

$$\sum_{k=0}^{K-1} \left( \frac{1}{2\pi} \int_{-\Omega}^{\Omega} |S(\omega_0)|^2 e^{i\omega_0(k-l)T} d\omega_0 \right) \alpha(\omega, t_k) = |S(\omega)|^2 e^{-i\omega lT}, \quad (21b)$$

where  $|S(\omega)|^2$  is the signal model power at  $\omega_0 = \omega$ . The system of linear equations (21b) is applicable for uniformly sampled signal  $x(kT)$  and can be derived from (9c) in a similar way as (21a).

The EDTFT basis  $\alpha(\omega, t_k)$  or  $\alpha(\omega, kT)$  can be found by applying different solution algorithms to the system of linear equations (21). In general, basis  $\mathbf{A}_\omega (K \times 1)$  is obtained in the matrix form as

$$\mathbf{A}_\omega = |S(\omega)|^2 \mathbf{R}^{-1} \mathbf{E}_\omega \quad (22)$$

and inserting (22) into expressions (5) and (10) yields the formulas for calculation of the EDTFT

$$F_\alpha(\omega) = \mathbf{x}\mathbf{A}_\omega = |S(\omega)|^2 \mathbf{x}\mathbf{R}^{-1} \mathbf{E}_\omega, \quad -\Omega \leq \omega \leq \Omega, \quad (23.1)$$

$$x_\alpha(t) = \mathbf{x}\mathbf{R}^{-1}\mathbf{E}_t, \quad -\infty < t < \infty, \quad (23.2)$$

$$S_\alpha(\omega) = \frac{\mathbf{x}\mathbf{A}_\omega}{\mathbf{E}_\omega^H\mathbf{A}_\omega} = \frac{\mathbf{x}|S(\omega)|^2\mathbf{R}^{-1}\mathbf{E}_\omega}{\mathbf{E}_\omega^H|S(\omega)|^2\mathbf{R}^{-1}\mathbf{E}_\omega} = \frac{\mathbf{x}\mathbf{R}^{-1}\mathbf{E}_\omega}{\mathbf{E}_\omega^H\mathbf{R}^{-1}\mathbf{E}_\omega}. \quad (23.3)$$

The elements of the matrices  $\mathbf{R}$  ( $K \times K$ ) and  $\mathbf{E}_t$  ( $K \times 1$ ) in the formulas (22, 23) are expressed by integrals

$$r_{l,k} = \frac{1}{2\pi} \int_{-\Omega}^{\Omega} |S(\omega_0)|^2 e^{i\omega_0(t_k-t_l)} d\omega_0 \quad \text{or} \quad r_{l,k} = \frac{1}{2\pi} \int_{-\Omega}^{\Omega} |S(\omega_0)|^2 e^{i\omega_0(k-l)T} d\omega_0, \quad (24.1)$$

$$e_l = \frac{1}{2\pi} \int_{-\Omega}^{\Omega} |S(\omega)|^2 e^{i\omega(t-t_l)} d\omega \quad \text{or} \quad e_l = \frac{1}{2\pi} \int_{-\Omega}^{\Omega} |S(\omega)|^2 e^{i\omega(t-lT)} d\omega, \quad (24.2)$$

for nonuniformly or uniformly sampled signal cases, respectively. If the signal and its model power spectra are close,  $|S_\alpha(\omega_0)|^2 \approx |S(\omega_0)|^2$ , then (24.1) is also an estimate of the autocorrelation function of the sequence  $\mathbf{x}$ . The inverse transform (23.2) calculated on time moments  $t=t_k$  or  $t=kT$ ,  $k=0,1,2,\dots,K-1$ , returns back the input sequence  $\mathbf{x}$  undistorted, as the elements of matrices  $\mathbf{E}_t$  become equal to  $\mathbf{R}$ . Case signal model  $S(\omega)=1$  the formulas (22) and (23) reduce to (16) and (17). The frequency resolution of the EDTFT is in inverse ration to  $|S(\omega)|^2\mathbf{E}_\omega^H\mathbf{R}^{-1}\mathbf{E}_\omega$  and varied in the frequency range  $-\Omega \leq \omega \leq \Omega$ .

### 3.3.3 Iterative EDTFT algorithm

Calculation of the EDTFT by formulas (23) requires knowledge of the signal model spectrum which generally is not known. At the same time, the amplitude spectrum obtained in the previous section according to formula (17.3) can be used as a source of such information. This suggests the following iterative algorithm introduced in [5], where the spectrum  $S(\omega)$  of signal model tends to the signal spectrum  $S_\alpha(\omega)$ :

*Iteration 1:* Calculate  $S_\alpha^{(1)}(\omega)$  (17.3) applying default signal model  $S(\omega)=1$ .

*Iteration 2:* Calculate  $S_\alpha^{(2)}(\omega)$  (23.3) by using the signal model  $S_\alpha^{(1)}(\omega_0)$ .

*Iteration 3:* Calculate  $S_\alpha^{(3)}(\omega)$  (23.3) by using the signal model  $S_\alpha^{(2)}(\omega_0)$ .

...

*Iteration it:* Calculate  $S_\alpha^{(it)}(\omega)$  (23.3) by using the signal model  $S_\alpha^{(it-1)}(\omega_0)$ .

The iterations are repeated until the given maximum iteration number is reached or the power spectrum does not alter from iteration to iteration,  $|S_\alpha^{(it)}(\omega)|^2 \approx |S_\alpha^{(it-1)}(\omega)|^2$ .

The EDTFT output  $F_\alpha(\omega)$  (23.1) is calculated for the last performed iteration.

By default, the signal model  $S(\omega)=1$  is used as input for the EDTFT algorithm. However, additional information about the signal to be analyzed can be applied to create a more realistic signal model for the EDTFT input and reduce the number of iterations required to reach the stop iteration criteria.

## 4 Extended DFT

EDTFT considered in the previous section is a function of the continuous frequency ( $-\Omega \leq \omega \leq \Omega$ ), while describing below EDFT algorithm calculate EDTFT on a discrete frequency set,  $-\Omega \leq \omega_n < \Omega$  for  $n=0,1,2,\dots,N-1$ . The number of frequency points  $N \geq K$  and it should be selected sufficiently great to substitute the integrals (24.1) used for calculation of the matrix  $\mathbf{R}$  ( $K \times K$ ) in the expressions (22, 23) by the finite sums

$$r_{l,k} = \frac{1}{2\pi} \int_{-\Omega}^{\Omega} |S(\omega_0)|^2 e^{i\omega_0(t_k-t_l)} d\omega_0 \approx \frac{\Omega}{\pi N} \sum_{n=0}^{N-1} |S(\omega_n)|^2 e^{i\omega_n(t_k-t_l)}, \quad (25.1)$$

$$r_{l,k} = \frac{1}{2\pi} \int_{-\Omega}^{\Omega} |S(\omega_0)|^2 e^{i\omega_0(k-l)T} d\omega_0 \approx \frac{\Omega}{\pi N} \sum_{n=0}^{N-1} |S(\omega_n)|^2 e^{i\omega_n(k-l)T}, \quad (25.2)$$

where  $l,k=0,1,2,\dots,K-1$ . The matrices composed of (25.1) and (25.2),

$$\mathbf{R} = \begin{bmatrix} r_{0,0}(0) & r_{0,1}(t_1 - t_0) & \cdots & r_{0,K-1}(t_{K-1} - t_0) \\ r_{1,0}(t_0 - t_1) & r_{1,1}(0) & \cdots & r_{1,K-1}(t_{K-1} - t_1) \\ \vdots & \vdots & \ddots & \vdots \\ r_{K-1,0}(t_0 - t_{K-1}) & r_{K-1,1}(t_1 - t_{K-1}) & \cdots & r_{K-1,K-1}(0) \end{bmatrix}, \quad (26.1)$$

$$\mathbf{R} = \begin{bmatrix} r_{0,0}(0) & r_{0,1}(T) & \cdots & r_{0,K-1}((K-1)T) \\ r_{1,0}(-T) & r_{1,1}(0) & \cdots & r_{1,K-1}((K-2)T) \\ \vdots & \vdots & \ddots & \vdots \\ r_{K-1,0}(-(K-1)T) & r_{K-1,1}(-(K-2)T) & \cdots & r_{K-1,K-1}(0) \end{bmatrix}, \quad (26.2)$$

possess Hermitian symmetry,  $r_{l,k} = r_{k,l}^*$ , but (26.2) for a uniformly sampled signal has also a Toeplitz structure. The matrix elements  $r_{l,k}$  represents the autocorrelation function and can be calculated by applying the IDFT to the signal model power spectrum  $|S(\omega_n)|^2$ . The frequency  $\Omega/\pi = 2f_u = f_N$  in (25), where  $f_u$  is the signal upper frequency and  $f_N$  is the Nyquist rate of a band-limited signal, and it is assumed to be normalized (equal to 1) in DFT calculations. The choice of frequencies  $\{\omega_n\} = \{2\pi f_n\}$  depends on the number of frequencies required for accurate estimation of (25) and detailed representation of the signal spectrum, as well as on the limitations of the total amount of calculations. Eventually, the uniform set of frequencies in range  $[-\Omega; \Omega]$  is preferable in most application cases.

The EDFT may be expressed by the iterative algorithm

$$\mathbf{R}^{(it)} = \frac{1}{N} \mathbf{E} \mathbf{W}^{(it)} \mathbf{E}^H, \quad (27.1)$$

$$\mathbf{F}^{(it)} = \mathbf{x} \mathbf{A}^{(it)} = \mathbf{x} (\mathbf{R}^{(it)})^{-1} \mathbf{E} \mathbf{W}^{(it)}, \quad (27.2)$$

$$\mathbf{S}^{(it)} = \frac{\mathbf{x} (\mathbf{R}^{(it)})^{-1} \mathbf{E}}{\text{diag}(\mathbf{E}^H (\mathbf{R}^{(it)})^{-1} \mathbf{E})}, \quad (27.3)$$

$$\mathbf{W}^{(it+1)} = \text{diag}(|\mathbf{S}^{(it)}|^2), \quad (27.4)$$

for iteration number  $it=1,2,3,\dots,I$ , wherein (27.1) is the sum (25) in matrix form. The matrix  $\mathbf{E}$  ( $K \times N$ ) has elements  $e^{-i2\pi f_n t_k}$  or  $e^{-i2\pi f_n kT}$  case sampling of  $\mathbf{x}$  done uniformly. By default, the diagonal weight matrix  $\mathbf{W}^{(it)}$  ( $N \times N$ ) for the first iteration is a unit matrix,  $\mathbf{W}^{(1)} = \mathbf{I}$ . If the other diagonal matrix is used as input to the EDFT algorithm, it should have at least  $K$  non-zero elements for stable output. In the next iterations  $\mathbf{W}^{(it+1)}$  is filled with power spectrum values calculated by (27.4). There may be additional criteria for stopping iterations before reaching the maximum number of iterations  $I$ , for example, iterations can be interrupted if the relative change in the power spectrum  $|\text{sum}(\mathbf{W}^{(it+1)}) - \text{sum}(\mathbf{W}^{(it)})| / \text{sum}(\mathbf{W}^{(2)})$  for  $it > 1$  is less than the specified threshold.

IDFT can be applied to output  $\mathbf{F}$  of each iteration and returns original  $K$  samples of uniform or nonuniform sequence

$$\mathbf{x} = \frac{1}{N} \mathbf{F} \mathbf{E}^H. \quad (28)$$

Since the length of the frequency set  $N \geq K$ , then (28) could be modified to obtain an extrapolated sequence  $\mathbf{x}_\alpha$  ( $1 \times N$ ) -  $x_\alpha(t_m)$  or  $x_\alpha(mT)$ ,  $m=0,1,2,\dots,N-1$ ,

$$\mathbf{x}_\alpha = \frac{1}{N} \mathbf{F} \mathbf{E}_N^H, \quad (29)$$

where exponents matrix  $\mathbf{E}_N$  ( $N \times N$ ) has elements  $e^{-i2\pi f_n t_m}$  or  $e^{-i2\pi f_n mT}$  case of uniform  $\mathbf{x}_\alpha$ , and  $\mathbf{x}\mathbf{x}^H \leq \mathbf{x}_\alpha \mathbf{x}_\alpha^H = \frac{1}{N} \mathbf{F}\mathbf{F}^H$  according to Parseval-Plancherel theorem. Reconstructed by the formula (29) sequence is the original sequence plus forward and backward extrapolation of  $\mathbf{x}$  to length  $N$  and/or interpolation if there are gaps inside of  $\mathbf{x}$ . The maximum frequency resolution is limited by the length  $N$  of frequency set, not by the length  $K$  of sequence  $\mathbf{x}$  as in the application of classical DFT. It means, the EDFT can increase the frequency resolution  $N/K$  times in comparison with the classical DFT. This can be verified by comparing the diagonal elements of the product of IDFT and DFT basis  $\text{diag}\left(\frac{1}{N} \mathbf{E}^H \mathbf{E}\right)$ , which are equal to  $K/N$  at all frequencies, with the relationship  $0 < \text{diag}\left(\frac{1}{N} \mathbf{E}^H \mathbf{A}\right) = \frac{1}{N} \mathbf{F}./\mathbf{S} \leq 1$  corresponding to the IDFT and EDFT basis  $\mathbf{A}$  (27.2). However, there is a restriction on the sum of frequency resolutions  $\text{sum}(\mathbf{F}./\mathbf{S})=NK$  satisfied by each iteration, and in order to achieve high resolution at certain frequencies, the EDFT must reduce the resolution at other frequencies. The deviation  $|\text{sum}(\mathbf{F}./\mathbf{S})-NK|$  can also be used as an additional criterion for stopping iterations, since it indicates the possible inaccuracy of the obtained results, caused mainly by the finite precision in calculations. If this happens, the result of the previous EDFT iteration should be considered as a final one.

In a border-case  $N=K$ , the iterative algorithm output does not depend on weight matrix  $\mathbf{W}$  and the optimal EDFT basis is found in a non-iterative way (in a result of the first iteration) [7].

## 5 EDFT and other nonparametric approaches

In the previous sections, starting with the Fourier integral (1) and using its orthogonality property (2), constructing and solving the minimum least squares error estimators (9), the Extended DFT was obtained analytically. In the following, a comparison will be made with known nonparametric approaches - Capon filter, Generalized (Weighted) Least Squares (GWLS) solution and High-Resolution Discrete Fourier Transform (HRDFT) introduced by Sacchi, Ulrych and Walker in 1998. The ways and opportunities of derivation an iterative EDFT algorithm based on these methods are analyzed briefly.

### 5.1 Capon filter approach

The Capon filter known also as Minimum Variance spectral estimate (see [3, 10, 11, 24]) can be viewed as the output of a bank of filters with each filter centered at one of the analyzes frequencies

$$y_\omega(nT) = \sum_{k=0}^{K-1} x((n-k)T) h_\omega(kT) = \tilde{\mathbf{x}} \mathbf{h}_\omega, \quad n = 0, 1, 2, \dots \quad (30)$$

In the matrix notation  $\tilde{\mathbf{x}} = [x(nT), x((n-1)T), \dots, x((n-K+1)T)]$  is the filter input signal and  $\mathbf{h}_\omega = [h_\omega(0), h_\omega(T), \dots, h_\omega((K-1)T)]^T$  is the filter coefficients. Here the subscript  $\omega$  indicate a dependence on the filter's center frequency.

The Capon filter is designed to minimize the variance on the filter output

$$\begin{aligned} \sigma_y^2 &= \mathcal{E}\{|y_\omega(nT)|^2\} = \mathcal{E}\{y_\omega^H(nT)y_\omega(nT)\} = \mathcal{E}\{\mathbf{h}_\omega^H \tilde{\mathbf{x}}^H \tilde{\mathbf{x}} \mathbf{h}_\omega\} \\ &= \mathbf{h}_\omega^H \mathcal{E}\{\tilde{\mathbf{x}}^H \tilde{\mathbf{x}}\} \mathbf{h}_\omega = \mathbf{h}_\omega^H \mathbf{R}_x \mathbf{h}_\omega, \end{aligned} \quad (31)$$

subject to the constraint that its frequency response at the frequency of interest  $\omega$  has unity gain

$$H(\omega) = \sum_{k=0}^{K-1} h_\omega(kT) e^{-i\omega kT} = \mathbf{E}_\omega^T \mathbf{h}_\omega = 1, \quad (32.1)$$

$$H(\omega) = \sum_{k=0}^{K-1} h_\omega^*(kT) e^{i\omega kT} = \mathbf{h}_\omega^H \mathbf{E}_\omega^* = 1, \quad (32.2)$$

Where  $\mathcal{E}\{\cdot\}$  denotes the expectation operator and the matrix  $\mathbf{E}_\omega$  ( $K \times 1$ ) has elements  $e^{-i\omega kT}$ . The constraints (32.1) and (32.2) must be satisfied by filter (30) and Hermitian transpose filter

$y_\omega^H(nT) = \mathbf{h}_\omega^H \tilde{\mathbf{x}}^H$ , correspondingly. The matrix  $\mathbf{R}_x = \mathbf{E}\{\tilde{\mathbf{x}}^H \tilde{\mathbf{x}}\}$  ( $K \times K$ ) is the sample autocorrelation matrix and it can be composed of the values of the signal autocorrelation function. For example, so called biased estimate is calculated by

$$r_{xx}(lT) = \frac{1}{K} \sum_{k=0}^{K-l-1} x((k+l)T) x^*(kT), \quad l = 0, 1, 2, \dots, K-1, \quad (33)$$

and, considering that  $r_{xx}(-lT) = r_{xx}^*(lT)$ , the sample autocorrelation matrix is filled as

$$\mathbf{R}_x = \begin{bmatrix} r_{0,0}(0) & r_{0,1}(-T) & \dots & r_{0,K-1}(-(K-1)T) \\ r_{1,0}(T) & r_{1,1}(0) & \dots & r_{1,K-1}(-(K-2)T) \\ \vdots & \vdots & \ddots & \vdots \\ r_{K-1,0}((K-1)T) & r_{K-1,1}((K-2)T) & \dots & r_{K-1,K-1}(0) \end{bmatrix}. \quad (34)$$

Mathematically, the Capon filter coefficients can be obtained by minimizing the variance (31) under the constraints given by (32.1) and (32.2)

$$J = \mathbf{h}_\omega^H \mathbf{R}_x \mathbf{h}_\omega - \mu(\mathbf{E}_\omega^T \mathbf{h}_\omega - 1) - \lambda(\mathbf{h}_\omega^H \mathbf{E}_\omega^* - 1) \rightarrow \min, \quad (35)$$

where  $\mu, \lambda$  are Lagrange multipliers. The conditions  $\frac{\partial J}{\partial \mathbf{h}_\omega} = 0$  and  $\frac{\partial J}{\partial \mathbf{h}_\omega^H} = 0$  must be fulfilled to determine the minimum of (35). Both requirements lead to the same solution

$$\mathbf{h}_\omega = \frac{\mathbf{R}_x^{-1} \mathbf{E}_\omega^*}{\mathbf{E}_\omega^T \mathbf{R}_x^{-1} \mathbf{E}_\omega^*} \quad (36)$$

and, traditionally, the Capon power spectrum is computed as

$$P_{Capon}(\omega) = \mathbf{h}_\omega^H \mathbf{R}_x \mathbf{h}_\omega = \frac{1}{\mathbf{E}_\omega^T \mathbf{R}_x^{-1} \mathbf{E}_\omega^*}. \quad (37)$$

To obtain an iterative EDFT algorithm from the original Capon filter approach, the sample autocorrelation matrix  $\mathbf{R}_x$  (34) must be substituted by  $\mathbf{R}^T = \mathbf{E}^* \mathbf{W} \mathbf{E}^T$ . The matrix  $\mathbf{R}^T$  ( $K \times K$ ) can also be obtained as a transpose of the EDFT matrix  $\mathbf{R}$  defined by (26). The elements of quadratic diagonal matrix  $\mathbf{W}$  ( $N \times N$ ) represent an estimate of power at time moment  $nT=0$ , determined from one sample at output of each Capon filter

$$|y_\omega(0)|^2 = |\tilde{\mathbf{x}} \mathbf{h}_\omega|^2 = \left| \frac{\tilde{\mathbf{x}} (\mathbf{R}^T)^{-1} \mathbf{E}_\omega^*}{\mathbf{E}_\omega^T (\mathbf{R}^T)^{-1} \mathbf{E}_\omega^*} \right|^2 \quad (38)$$

where the filter input sequence  $\tilde{\mathbf{x}}$  (30) is related to the EDFT input sequence  $\mathbf{x}$  as  $\tilde{x}(kT) = x((K+k-1)T)$  or  $\tilde{x}(t_k) = x(t_{K+k-1})$ ,  $k=0, -1, -2, \dots, -(K-1)$ , for uniformly or nonuniformly sampled sequence cases, respectively.

Eventually, an iterative algorithm can be formed as follows

$$\mathbf{R}^{T(it)} = \mathbf{E}^* \mathbf{W}^{(it)} \mathbf{E}^T, \quad (39.1)$$

$$\mathbf{S}_{Capon}^{(it)} = \frac{\tilde{\mathbf{x}} (\mathbf{R}^{T(it)})^{-1} \mathbf{E}_\omega^*}{\text{diag}(\mathbf{E}^T (\mathbf{R}^{T(it)})^{-1} \mathbf{E}_\omega^*)}, \quad (39.2)$$

$$\mathbf{W}^{(it+1)} = \text{diag} \left( \left| \mathbf{S}_{Capon}^{(it)} \right|^2 \right), \quad (39.3)$$

with the initial condition for  $\mathbf{W}^{(1)} = \mathbf{I}$  and the iteration number  $it=1, 2, 3, \dots, I$ . The estimate of the power spectrum  $\left| \mathbf{S}_{Capon}^{(it)} \right|^2$  coincides with the results of the EDFT, while the phase spectrum is different.

It should be noted that the calculation of the Capon filter output power by (37) is theoretically well justified, whereas the derivation of (39) requires *ad hoc* assumptions and substitutions and is a measurement of power obtained from just a one sample at the output of the filter. This leads to conclusion that the approach (39) is simply a filter-bank interpretation of the EDFT, similarly to the DFT which can also be considered as a bank of filters. In addition, an iterative algorithm derived based on Capon filter cannot reveal all the EDFT capacity, such as the ability to estimate DFT (27.2) and restore the signal (28, 29).

## 5.2 GWLS solution

The Generalized (Weighted) Least Squares approach (see [3, 15, 18, 34]) in the spectral analysis could be based on the following data model

$$\mathbf{x}^T = \mathbf{E}_\omega^* S_{GWLS}(\omega) + \mathbf{e}_Q, \quad (40)$$

with  $\mathbf{e}_Q$  denoting the noise and interference component, and  $\mathbf{E}_\omega^* S_{GWLS}(\omega)$  representing the signal component on the frequency of interest with unknown complex amplitude  $S_{GWLS}(\omega)$ . The GWLS minimizes

$$[\mathbf{x}^T - \mathbf{E}_\omega^* S_{GWLS}(\omega)]^H \mathbf{Q}^{-1} [\mathbf{x}^T - \mathbf{E}_\omega^* S_{GWLS}(\omega)], \quad (41)$$

which is solved by

$$S_{GWLS}(\omega) = \frac{\mathbf{E}_\omega^T \mathbf{Q}^{-1} \mathbf{x}^T}{\mathbf{E}_\omega^T \mathbf{Q}^{-1} \mathbf{E}_\omega^*}, \quad (42)$$

where  $\mathbf{Q}$  ( $K \times K$ ) is the covariance matrix of the data model component  $\mathbf{e}_Q$ . There are two special cases of GWLS called Weighted Least Squares (WLS) and ordinary Least Squares (LS). WLS occur when all the off-diagonal entries of  $\mathbf{Q}$  are 0, while LS solution is obtained from the GWLS under the assumption that  $\mathbf{e}_Q$  at (40) is a white noise, hence  $\mathbf{Q}=\mathbf{I}$ .

The problem of GWLS estimator is that, in general, the noise covariance matrix  $\mathbf{Q}$  is not known, and must be estimated from the data along with the  $S_{GWLS}(\omega)$ . The initial estimate (the 1<sup>st</sup> iteration) could be equal to LS solution, it is (42) with  $\mathbf{Q}=\mathbf{I}$ . Next, to ensure that the GWLS solution works in an iterative way as EDTFT do, the noise covariance matrix should be calculated as  $\mathbf{Q} = \mathbf{R}^T = \mathbf{E}^* \mathbf{W} \mathbf{E}^T$  under the assumption  $\mathbf{W} = \text{diag}(|S_{GWLS}(\omega)|^2)$ . As a result, the GWLS solution (42) coincides with the EDTFT formula (23.3)

$$S_{GWLS}(\omega) = \frac{\mathbf{E}_\omega^T (\mathbf{R}^T)^{-1} \mathbf{x}^T}{\mathbf{E}_\omega^T (\mathbf{R}^T)^{-1} \mathbf{E}_\omega^*} = \frac{\mathbf{x} \mathbf{R}^{-1} \mathbf{E}_\omega}{\mathbf{E}_\omega^H \mathbf{R}^{-1} \mathbf{E}_\omega} = S_\alpha(\omega) \quad (43)$$

and, as shown in Section 3.3.3, can be successfully used to iteratively update the amplitude spectrum.

Although substitution of a noise covariance matrix by  $\mathbf{R}^T$  is straightforward, it is not supported by GWLS data model (40), from which the matrix  $\mathbf{Q}$  represents only the model component  $\mathbf{e}_Q$  and the signal component  $\mathbf{E}_\omega^* S_{GWLS}(\omega)$  must be excluded from it, while the matrix  $\mathbf{R}^T$  is calculated for the entire signal  $\mathbf{x}^T$  including  $\mathbf{e}_Q$  and  $\mathbf{E}_\omega^* S_{GWLS}(\omega)$ . Consequently,  $S_{GWLS}(\omega)$  shows all components of data in the frequency domain, including noise. Furthermore, the signal is restored by applying IDFT (28) to the Extended Fourier transform  $\mathbf{F}$ ,  $\mathbf{x}^T = \frac{1}{N} \mathbf{E}^* \mathbf{F} \neq \mathbf{E}^* \mathbf{S}$ , and not as an inverse of the Amplitude spectrum  $\mathbf{S}$  as it is assumed in (40). Using an estimate  $S_{GWLS}(\omega)=S_\alpha(\omega)$  in the data model leads to a predetermined split of the signal at frequency  $\omega$  in between both components, where the noise part expressed as  $\mathbf{e}_Q = \frac{1}{N} \mathbf{E}^* \mathbf{F} - \mathbf{E}^* \mathbf{S}$ . The conclusion is that there is a discrepancy between predicted result by the model and the result obtained by (43). Model (40) serves as an interpretation that can be successfully applied to the EDTFT output in the special case where noise spectrum is spread over the entire frequency range, but the signal spectrum is highly localized, as will be shown in Computer simulations section.

## 5.3 High-Resolution DFT

The third method considered here is High-Resolution DFT proposed by Sacchi, Ulrych and Walker in [9]. The authors presented an iterative nonparametric approach of spectral estimation, which minimizes the cost function deduced from Bayes' theorem and, as well as Extended DFT, makes it possible to obtain high-resolution Fourier spectrum. The HRDFT algorithm can be reduced to the following iterative procedure:

$$\mathbf{R}^{(it)} = \frac{1}{N} \mathbf{E} \mathbf{W}^{(it)} \mathbf{E}^H, \quad (44.1)$$

$$\mathbf{F}_{HRDFT}^{(it)} = \mathbf{x}(\mathbf{R}^{(it)})^{-1} \mathbf{E} \mathbf{W}^{(it)}, \quad (44.2)$$

$$\mathbf{W}^{(it+1)} = \text{diag} \left( \left| \frac{1}{N} \mathbf{F}_{HRDFT}^{(it)} \right|^2 \right) \quad (44.3)$$

for iteration number  $it=1,2,3,\dots,I$  and with the initial condition  $\mathbf{W}^{(1)}=\mathbf{I}$ .

The IDFT (28) applied to any iteration output (44.2) returns the sequence  $\mathbf{x}$  undistorted. The main difference between approaches is that the HRDFT algorithm lack of formula to estimate of amplitude spectrum (27.3). Instead, as input for the next iteration, it uses the Fourier spectrum estimated in the previous iteration. Thus, the results of HRDFT differ from output of EDFT significantly. HRDFT iterates to the solution where the signal is approximated by  $K$  frequencies while the power on other  $N-K$  frequencies becomes negligible. Each valuable frequency is resolved with maximum resolution restricted by the length of HRDFT. Also, it still obeys the same limit on the sum of resolutions by frequency ( $KN$ ) as DFT and EDFT.

The authors [39] investigated algorithms with weights different from (44.3) for adaptation the correlation matrix (44.1), although only the amplitude spectrum (10) derived accordingly to the minimum least squares expression (9) and calculated by (27.4) fits perfectly to an iterative update of the matrix  $\mathbf{R}$  and returns results that are closest to the Fourier transform in the  $L^2$ -norm sense.

## 6 Computer simulations

The EDFT algorithm is validated on the data which are similar to those that have been used in [5, 7, 8]. The true spectrum of the first test signal consists of a band-limited noise (flat) in the frequency range  $[-0.5\dots-0.25]$  Hz, a rectangular pulse in the range  $[0\dots0.25]$  Hz and two unit-power complex exponents at frequencies 0.35 Hz and 0.3985 Hz. These three components represent random, transient pulse and deterministic parts of a composite signal with the upper frequency  $f_u=0.5$  Hz. Uniform and nonuniform sequences of the length  $K=64$  samples are derived by simulating 10-bit Analog-to-Digital Converter (ADC). Sampling and mean sampling periods of both sequences are equal to 1 second,  $T=T_s=1$ s. Sampling time points for the nonuniform sequence are generated as,  $t_k=kT+\tau_k$ ,  $k=0,1,2,\dots,K-1$ , where  $\{\tau_k\}$  are uniformly distributed random values in the range  $[0\dots0.8$ s]. Thus, the true spectrum of complex valued sequences consists of three non-overlapping in frequency domain components and ADC added floor noise ( $\approx-60$ dB), and it is symbolized by red color lines in the Figures 1-5. Please note that the unit of time as a second and frequency unit as Hz was selected here only for demonstration purposes and convenience.

The plots in Figures 1 and 2 show the performance of EDFT (black lines) for uniform and nonuniform sequences and allows to compare it with the classical DFT (blue lines). The number of frequencies (the length of DFT) is chosen equal to  $N=1000$ , which gives spectral estimates with DFT frequency bin spacing  $2f_u/N=0.001$  Hz. This means that the range  $[-0.5\dots0.5]$  Hz is uniformly covered by frequencies and used for the calculations in (25, 27) and for the signal representation in the frequency domain (spectral plots). Figures 1a and 2a display the power spectra of EDFT calculated as  $10\log(|\mathbf{S}|^2)$  in a non-iterative way. The input matrix  $\mathbf{W}$  in this case is composed of values of the true spectrum (red line in the plots), therefore there is no need for further iterations. Non-iterative estimate is very close to the EDFT 15<sup>th</sup> iteration depicted in Figures 1b and 2b, where the matrix  $\mathbf{W}=\mathbf{I}$  used in the input and confirms the correctness of the iterative algorithm. Figures 1c and 2c show the Power Spectral Density (PSD) calculated by the EDFT as  $10\log(|\mathbf{F}|^2/N)$  and proves the expectations, that PSD estimate on a complex exponent should increase in a value in comparison with the classical DFT if the proposed method achieves a high resolution around this frequency.

Figure 1d and 2d plotting the relative frequency resolution for the EDFT 15<sup>th</sup> iteration calculated as  $\frac{1}{2f_uTK} \mathbf{F}./\mathbf{S}$  (1d) or  $\frac{1}{2f_uT_sK} \mathbf{F}./\mathbf{S}$  (2d) in respect to the DFT for which, in accordance with (18), it is simply equal to 1 at all frequencies. The value  $2f_uT=2f_uT_s=1$  and this means that the signal is

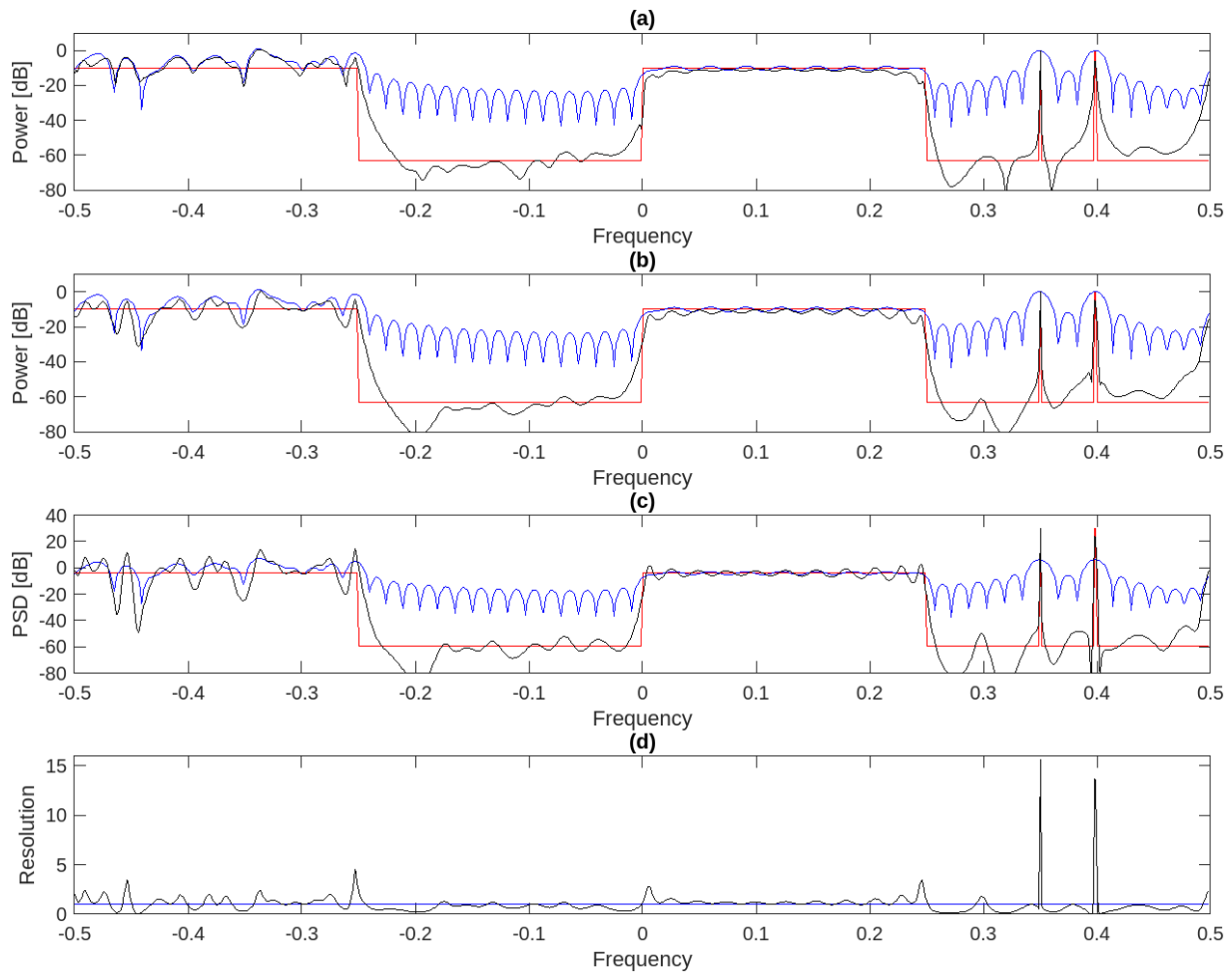


**Figure 1.** Uniform complex-valued sequence - the estimate of:  
**(a)** Power spectrum - True (red), DFT (blue) and non-iterative EDFT (black),  
**(b)** Power spectrum - True (red), DFT (blue) and EDFT (15<sup>th</sup> iteration, black),  
**(c)** Power Spectral Density - True (red), DFT (blue) and EDFT (15<sup>th</sup> iteration, black),  
**(d)** Relative frequency resolution - DFT (blue) and EDFT (15<sup>th</sup> iteration, black).

processed in one Nyquist zone. The DFT is showing a normal frequency resolution, whereas the EDFT have ability to increase the resolution (in plot appears values  $>1$ ) around the powerful signal components and decrease the resolution (in plot appears values  $<1$ ) at frequencies where the signal has weak power components. The EDFT is called as a high-resolution method and that is true, but with the following remark - it keeps the same 'summary' resolution as the traditional DFT or, in other words, squares under black and blue curves in Figure 1d (2d) are equal. The maximum frequency resolution is limited by value of division  $N/K$ . For example, if  $K=64$  and  $N=1000$ , then the EDFT can potentially improve the frequency resolution  $1000/64 \approx 16$  times. The peak resolution is achieved on a deterministic signal part - at frequency 0.35 Hz. The resolution of 0.3985 Hz exponent does not reach the maximum value because its frequency is not on EDFT grid (0.001 Hz) and the power is distributed among adjacent frequency bins. This is a known artifact of the DFT analysis and can be eliminated by using a finer frequency grid. Pulse signal ( $[0 \dots 0.25]$  Hz) is processed by EDFT with about the same resolution as DFT ( $\sim 1$ ). The relative resolution of random component ( $[-0.5 \dots -0.25]$  Hz) fluctuates around 1, while at frequencies where only ADC noise can be detected, EDFT reduces the frequency resolution below normal.

EDFT estimates in Figures 1 and 2 are close to each other and proves that the proposed approach can handle uniform and nonuniform sequences with the same quality, while the efficiency of classical DFT gets worse in case of nonuniform sequence. The simulation shows that EDFT can

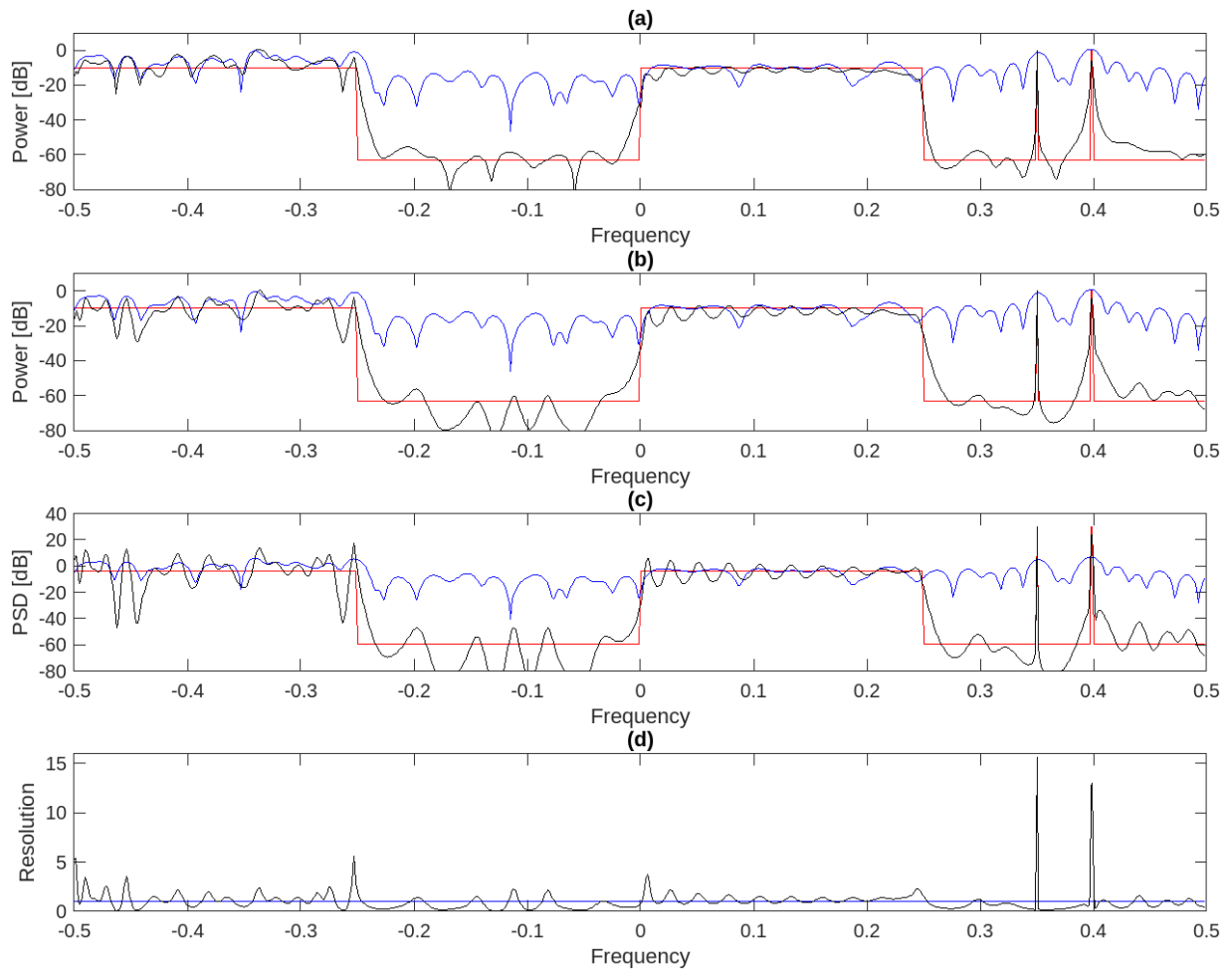


**Figure 2.** Nonuniform complex-value sequence - the estimate of:  
**(a)** Power spectrum - True (red), DFT (blue) and non-iterative EDFT (black),  
**(b)** Power spectrum - True (red), DFT (blue) and EDFT (15<sup>th</sup> iteration, black),  
**(c)** Power Spectral Density - True (red), DFT (blue) and EDFT (15<sup>th</sup> iteration, black),  
**(d)** Relative frequency resolution - DFT (blue) and EDFT (15<sup>th</sup> iteration, black).

successfully estimate random, transient and deterministic signal spectra and provide results superior to those produced by traditional DFT. The reason is that we have imposed a constraint on the DFT by padding the data with zeros beyond the 64-point sequence, even though we don't know how the sequence actually behaves there, whereas EDFT has no such restriction, hence we observe no sidelobes, eliminate frequency masking effects, and obtain higher frequency resolution.

Figure 3 compares classical DFT and EDFT estimates on nonuniform set of frequencies. The DFT bin spacing is randomized by adding values uniformly distributed in range  $\pm 0.0004$  Hz to uniform grid points. Figure 3a displays PSD of the same uniform sequence as in Figure 1c and revealing the similarity of both plots which is the expected result. Nonuniform frequency grid may affect the estimate of deterministic component of the test sequence. For example, the exponent at 0.3985 Hz in Figure 3a is closer to the randomized grid point while another one at 0.35 Hz will no longer there, causing the relative frequency resolution peak to be corrected for both exponents in Figure 3b. All of the above applies to the PSD estimate of nonuniform sequence on nonuniform set of frequencies shown in Figures 3c and 3d.

Figures 1-3 demonstrate the universality of EDFT and its broad applicability. The same algorithm handles uniform and nonuniform sequences equally well and provides high-resolution estimates on uniform or nonuniform frequency grid. However, introducing of nonuniformities reduces the possibility of using fast calculation algorithms inside EDFT and this factor should always be taken into account when choosing between a uniform or nonuniform approaches. Although there are

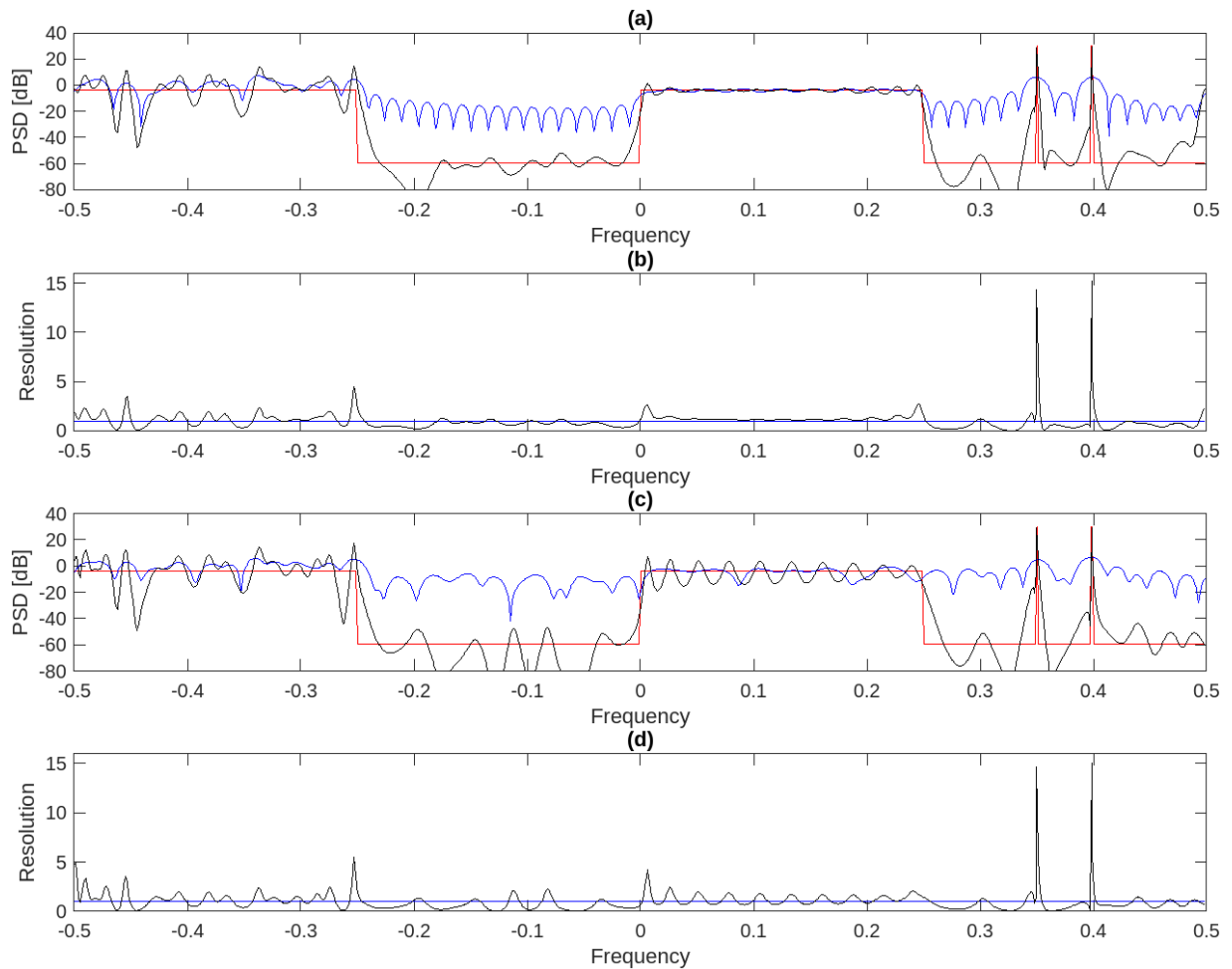


**Figure 3.** The estimate on nonuniform frequency set:

- (a) Power Spectral Density and (b) Relative frequency resolution of uniform sequence,
  - (c) Power Spectral Density and (d) Relative frequency resolution of nonuniform sequence:
- True (red), DFT (blue) and EDFT (15<sup>th</sup> iteration, black)

benefits that will be described in the following simulations.

Figure 4 explains the difference in performance between uniform and nonuniform inputs, where the spectra of both sequences are analyzed in the extended frequency range,  $[-1...1[$  Hz. The number of frequency points and the upper frequency are increased two times,  $N=2000$  and  $f_u=1$  Hz. This means that the step by frequency remains the same as in the Figures 1 and 2. The true spectrum of sequences at frequencies above 0.5 Hz consists only of floor noise ( $\approx -60$ dB) added by ADC. The actual result depicted in Figure 4a shows periodicity of the DFT and EDFT spectral estimates, which cannot be avoided for uniform sequences. In contrast, EDFT applied to the nonuniform sequence returns correct power spectrum in Figure 4b. Relative resolution of the nonuniform DFT in Figure 4c is calculated as  $1/(2f_u T_s)=0.5$  and it is half the normal resolution because of analysis is performed in two Nyquist zones. Nevertheless, squares under blue and black plots in Figure 4c are equal to one's depicted in Figure 2d. The maximum increase in the frequency resolution  $2000/64 \approx 31$  times is achieved on a complex exponent at frequency 0.35 Hz by the EDFT. The EDFT also increases resolution in half to process transient and random signal components with the normal frequency resolution equal to 1, as it is indicated by the red dotted lines in Figure 4c. Hence the conclusion that EDFT can handle nonuniformly sampled signals in multiple Nyquist zones only if the overall spectrum of band-limited signal components does not exceed one zone.

Since the spectrum of uniform sequence (red color line in Figure 1) does not cover the entire Nyquist zone EDFT should be able to handle it with mean sampling period  $T_s$  greater than  $T$  but

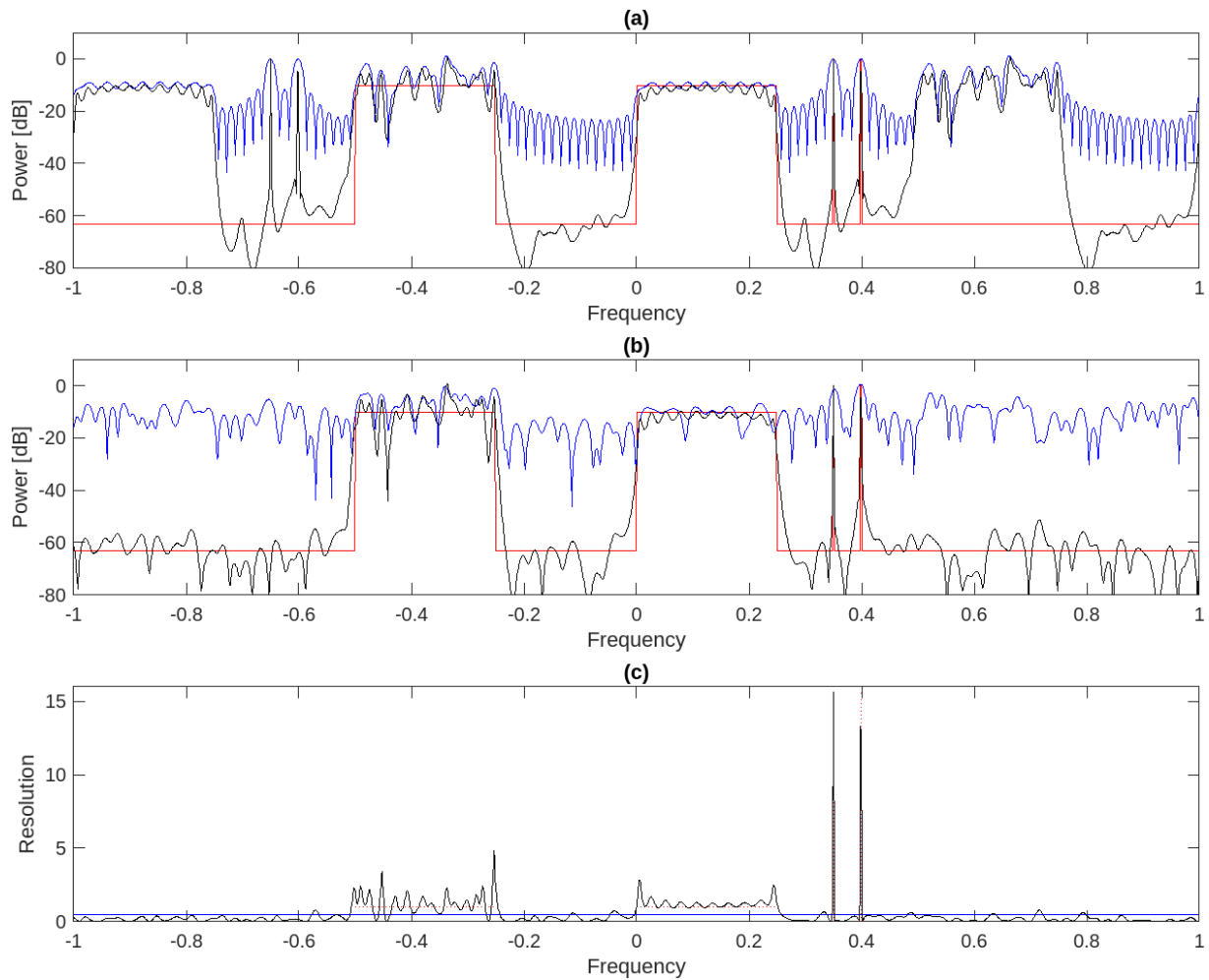


**Figure 4.** The estimates obtained in the extended frequency range:

(a) Power spectrum of uniform sequence, (b) Power spectrum of nonuniform, (c) Relative frequency resolution of nonuniform sequence: DFT (blue) and EDFT (black).

less than  $2T$ . The increase of  $T_s$  could be achieved by skipping samples from the uniform sequence randomly. The resulting sequence is considered as nonuniformly sampled because the distance between adjacent readings become unequal. The power spectra in Figure 5 show an example of the impact of sample skipping on the performance of DFT and EDFT. Input sequences are modeled by removing 16 and 24 samples randomly from the uniform 64-point data and leads to increase of mean sampling period  $T_s=64/48T=1,33s$  and  $T_s=64/40T=1,6s$ , respectively. The simulation shows that DFT fails to process sequences with missing samples, while EDFT is still applicable (Figure 5.b) if one Nyquist zone limit on the total signal component spectrum is satisfied, otherwise the estimate becomes worse (Figure 5.c). Note that the result depends not only on the number of skipped samples, but also on their distribution within the sequence. The most sensitive to missing samples are transient signals which require dense sampling within their location, whereas deterministic signals appear more resistant, especially if the frequencies of discrete components lie on the EDFT grid. It is expected that the considerably greater increase of mean sampling period  $T_s$  can be achieved for pure deterministic signals [7].

Let's validate the above expectations for a signal consisting only of sinusoids in white noise, and generate a real-value sequence of length  $K=64$  samples as the sum of four sine waves with predefined amplitudes 0.5, 1, 2 and 3, having arbitrary initial phases and randomly selected frequencies on the EDFT grid (0.001 Hz). Moreover, the signal is also sampled on  $T=1$  second grid by randomly selecting 64 time points in the interval  $NT=1000$  seconds, resulting in an approximately 16-fold increase of mean sampling period  $T_s=NT/K=15,625s$ .

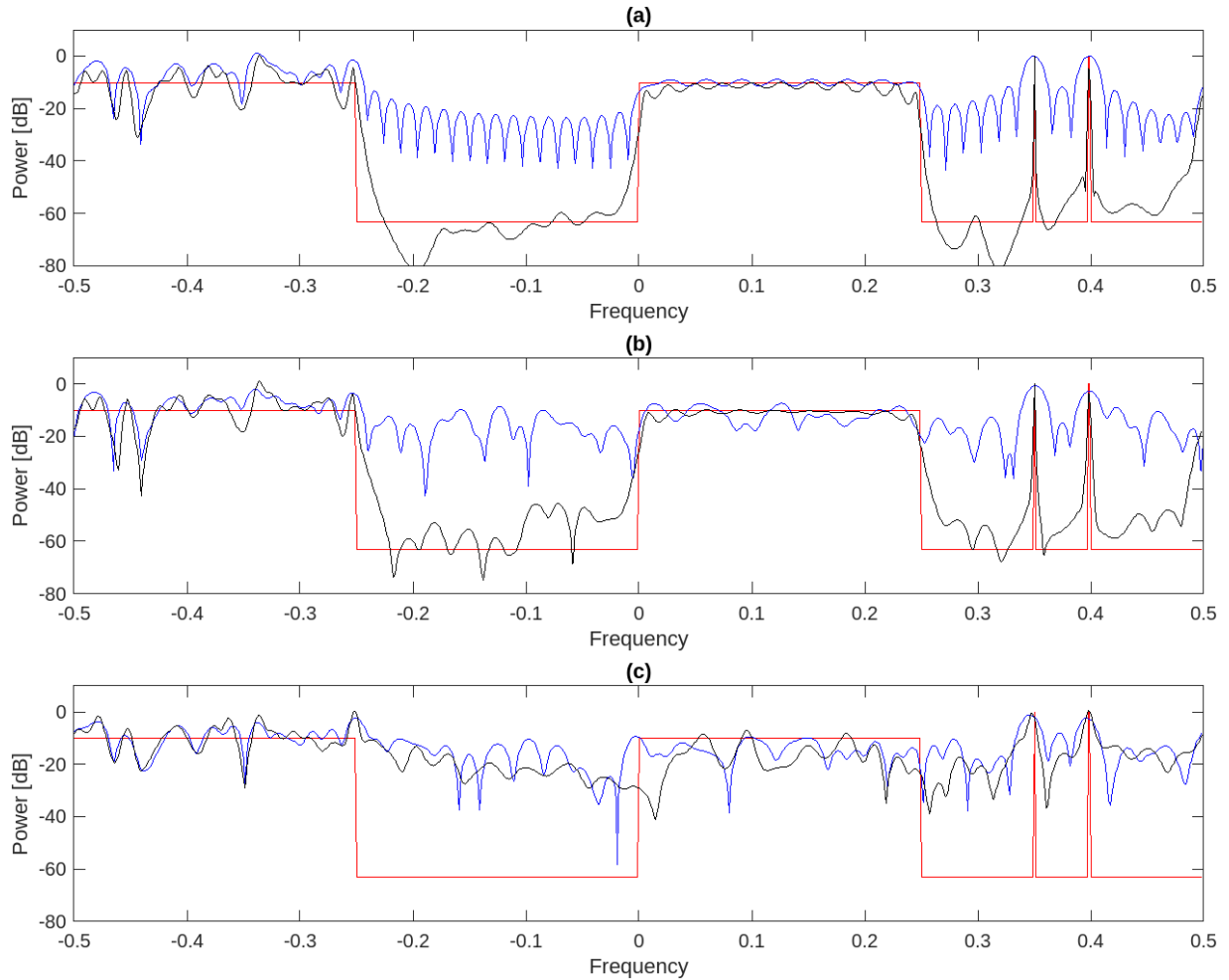


**Figure 5.** The power spectrum - True (red), DFT (blue) and EDFT (black), of the 64-point sequence without losses **(a)** and with randomly skipped **(b)** 16 and **(c)** 24 samples.

Finally, a white Gaussian noise with SNR=20 dB is added and nonuniform real-value sequence illustrated in Figure 6a. The true frequencies and amplitudes (red cycles) as well as the amplitude estimates of DFT (blue line) and EDFT (black line) are depicted in the Figure 6b and showed that DFT cannot recognize weaker power sinusoids while the EDFT picks up all of them and estimates their amplitudes and phases precisely. The performance difference is explained in the Figure 6c by comparison of the resolution of both DFTs with respect to the normal frequency resolution (equal to one). The relative resolution of the DFT (blue line) is calculated as  $1/(2f_u T_s) = K/N = 0.064$  and it is considerably less than it is required for successful signal processing. This causes aliasing and leakage effects, because the spectrum of the sequence spreading in almost 16 Nyquist zones and  $N-K$  samples at the input of the DFT could be considered as zeroed by the rectangular windows. The relative resolution of the EDFT (black line) is calculated as  $\frac{1}{2f_u T_s K} \mathbf{F} \cdot \mathbf{S} = \frac{1}{N} \mathbf{F} \cdot \mathbf{S}$  and it increases  $N/K$  times reaching the value close to one at frequencies of sinusoids. Thus, signal processing with just a normal frequency resolution allows EDFT not only estimate the parameters of the signal components correctly, but also IDFT applied to its output returns a sequence of length  $N$  consisting of the original  $K$  and  $N-K$  interpolated samples (see Figure 6d). It should be noted that only a deterministic part of the signal is interpolated by EDFT, whereas a white Gaussian noise stays localized in time around the sampling points (red cycles).

The next sequence used in the computer simulations is well-known Marple & Kay data set taken from [3]. It is 64-points real sample sequence of a process consisting of two-unit power sine waves with frequencies of 0.2 and 0.21 Hz, a third one with a power of 0.1 (20 dB down) at 0.1 Hz and a

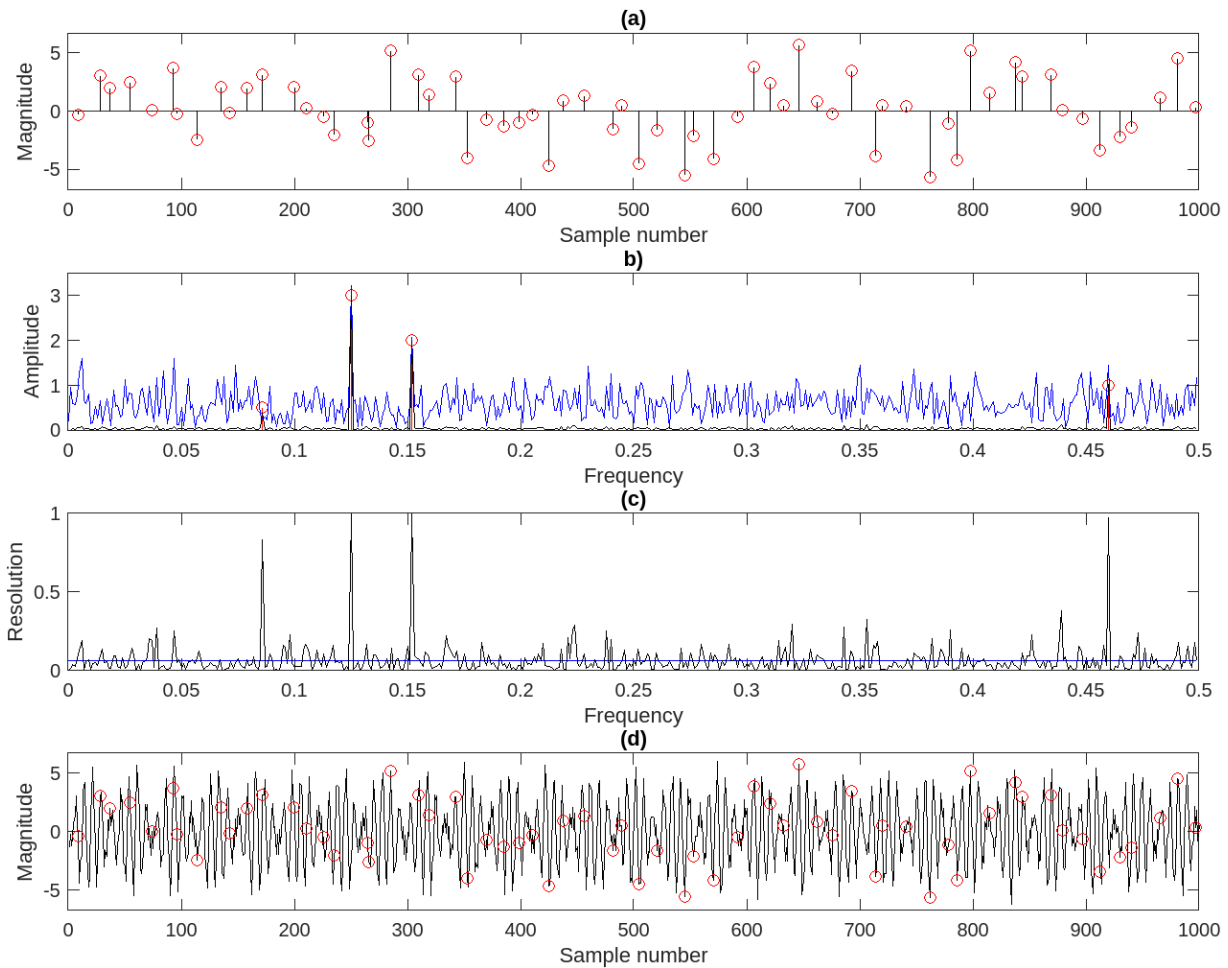


**Figure 6.** Real-value sequence (a) - 64 nonuniform samples, SNR 20 dB, Amplitude spectrum (b) - True values (red cycles) and estimates by DFT (blue), EDFT (black), Relative frequency resolution (c) by DFT (blue line) and EDFT (black), Original (blue cycles) and interpolated sequence (d) by Inverse EDFT - 1000 uniform samples.

colored noise in the frequency range  $[0.2 \dots 0.5]$  Hz (see red color lines in Figure 7). The signal upper frequency is  $f_i=0.5$  Hz and the length of the DFT is selected  $N=1000$ . Only 500 positive frequencies are displayed, because the sequence is a real-valued and negative frequencies, if they are depicted, gives a symmetrical pattern to zero frequency. The Figure 7 shows the power spectra of the DFT, EDFT and HRDFT approaches in a single picture, while separately, these plots have been presented in [5, 9]. The performance of other well-known spectral analysis methods for Marple & Kay data set could be found in [3], including Minimum Variance approach, named in the Section 5.1 as a traditional Capon filter (37). The simulation results in the Figure 7a,b demonstrate that the classical DFT and EDFT can evaluate not only the spectrum of sinusoids, but also the shape of continuous spectrum of other signal components, whereas HRDFT on Figure 7c is suitable mostly for the estimation of a line spectrum. The plot in Figure 7a shows that due to limited frequency resolution the classical DFT cannot resolve sine waves at the frequencies 0.2 and 0.21. Although the first EDFT iteration coincides with DFT, in the further iterations EDFT is able to increase the frequency resolution around the powerful signal components and all three sine waves are clearly distinguished after the 15<sup>th</sup> iteration in the Figure 7b.

All the three DFTs have one common feature - the ability to get back 64 samples of Marple & Kay data set by applying IDFT to the output of each of these methods. Since the length of the DFT is chosen equal to 1000, the inverse transform (29) returns 1000-64 additional samples, which are plotted in Figure 8 (black). The samples 65, 66, 67, ... are considered as a forward extrapolation but

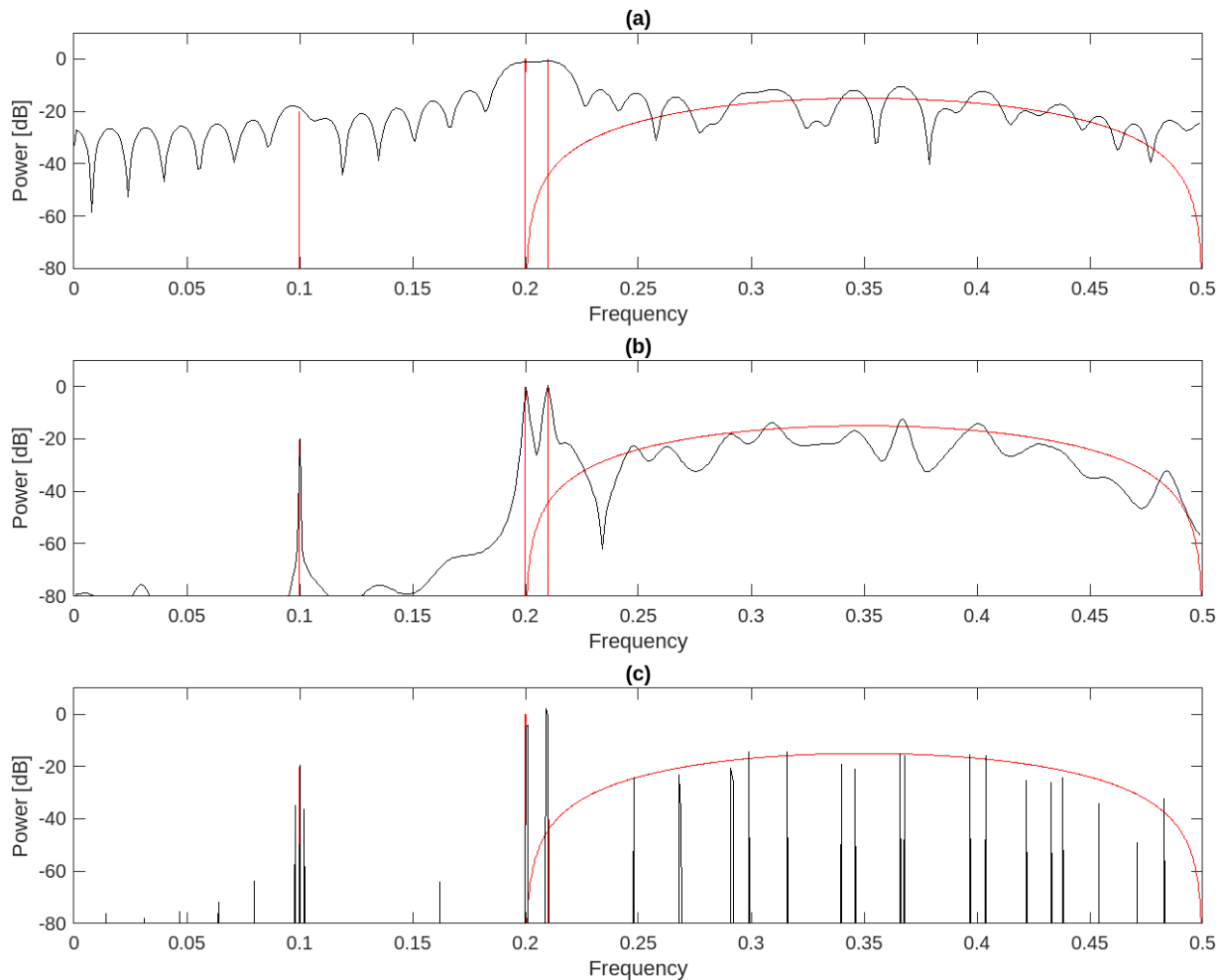


**Figure 7.** The power spectrum obtained for Marple & Kay data set by (a) DFT, (b) EDFT, (c) HRDFT.

samples 1000, 999, 998, ... as a backward extrapolation of known 64-sample sequence (blue). Of course, Marple & Kay sequence outside of giving data set is unknown and plots on Figure 8 are just three possible versions of its extrapolation. The classical DFT (Figure 8a) suggests that the sequence outside of given 64 samples will be zeros, HRDFT (Figure 8c) shows that the extrapolated data even will increase in power, while EDFT (Figure 8b) expects that the sequence beyond will have approximately the same power, which only gradually decreases in time. The way how the signal gets extrapolated by DFTs shows that the data is treated as lying on closed circle, where the first and last data samples are “neighbors”, that is, the space in time between them is equal to  $T$ . Increasing the length of DFT over the length of data allows extrapolation in both time directions. At the end of the computer modeling, we will examine the extrapolated sequences obtained at the output of IDFT if Marple & Kay data set is replaced by the same size white Gaussian noise (Figure 9). According to the theory the PSD of white Gaussian noise should be constant (flat) across the entire frequency range and the readings in a such sequence are uncorrelated random variables, therefore they cannot be extrapolated. In practice, because of finite length sequences and pseudo-random generators used in the simulations, the above expectations are satisfied only approximately. The classical DFT, like the Marple & Kay data illustrated in Figure 8a, also produces zeros outside the given sequence of 64 points in Figure 9a, which this time is completely consistent with the theory. Extrapolate by the EDFT (Figure 9b) vanish quickly, and this still agrees with the theory if practical considerations are taken into account. HRDFT (Figure 9c) in contrary to DFT and EDFT extends the white Gaussian noise up to a length of 1000 samples showing a strong correlation in the input sequence and this is very unlikely to be true.

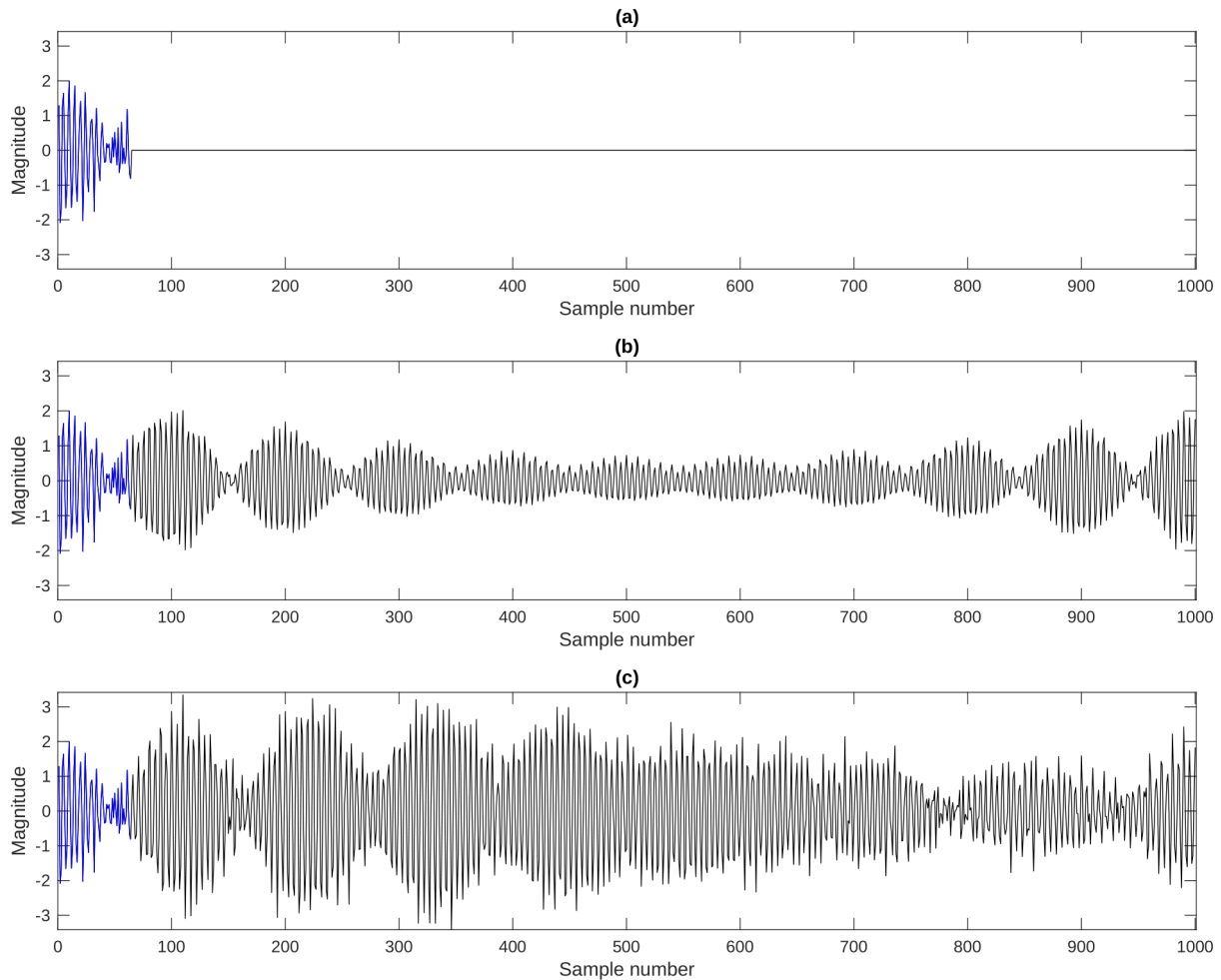


**Figure 8.** Marple & Kay sequence (blue) and extrapolated data (black) by inverse **(a)** DFT, **(b)** EDFT, **(c)** HRDFT.

## 7 Conclusion

Computer simulations revealed the key features of EDFT - the ability to process uniform and nonuniform data as long as the spectrum of data components does not exceed frequency range equivalent to one Nyquist zone. EDFT provides two properly scaled outputs, one proportional to the power spectral density and the other to the power of data components. This makes it possible to track the resolution achieved during the iteration process, which is proportional to the ratio of both outputs. It is shown that the maximum frequency resolution is limited by the length of DFT rather than the length of data as previously thought. Consequently, the inverse DFT applied to the output of EDFT returns not only input data undistorted but also extrapolates and interpolates the data along the length of the transform.

Any approach that claims that it is a high frequency resolution method in accordance with the Uncertainty Principle must make certain assumptions about data outside of the observation period even if by itself it is not able to recover the signal. An increase in resolution is dictated by well-known laws of physics, from where the longer data, the higher the resolution has been achieved. The advantage of proposed method over similar ones is that EDFT based on a solution that satisfies the minimum least squares criteria (6), making it an accurate, reliable and stable. Moreover, EDFT answers the question of what is DFT and how to obtain it in three cases: first, when the length of data is less than the size of transform, second, when there are missing readings or gaps in the data, and third, when data is nonuniform, that is, the distances between readings are not equal.

The next section will present MATLAB programs for computing EDFT for all three cases.

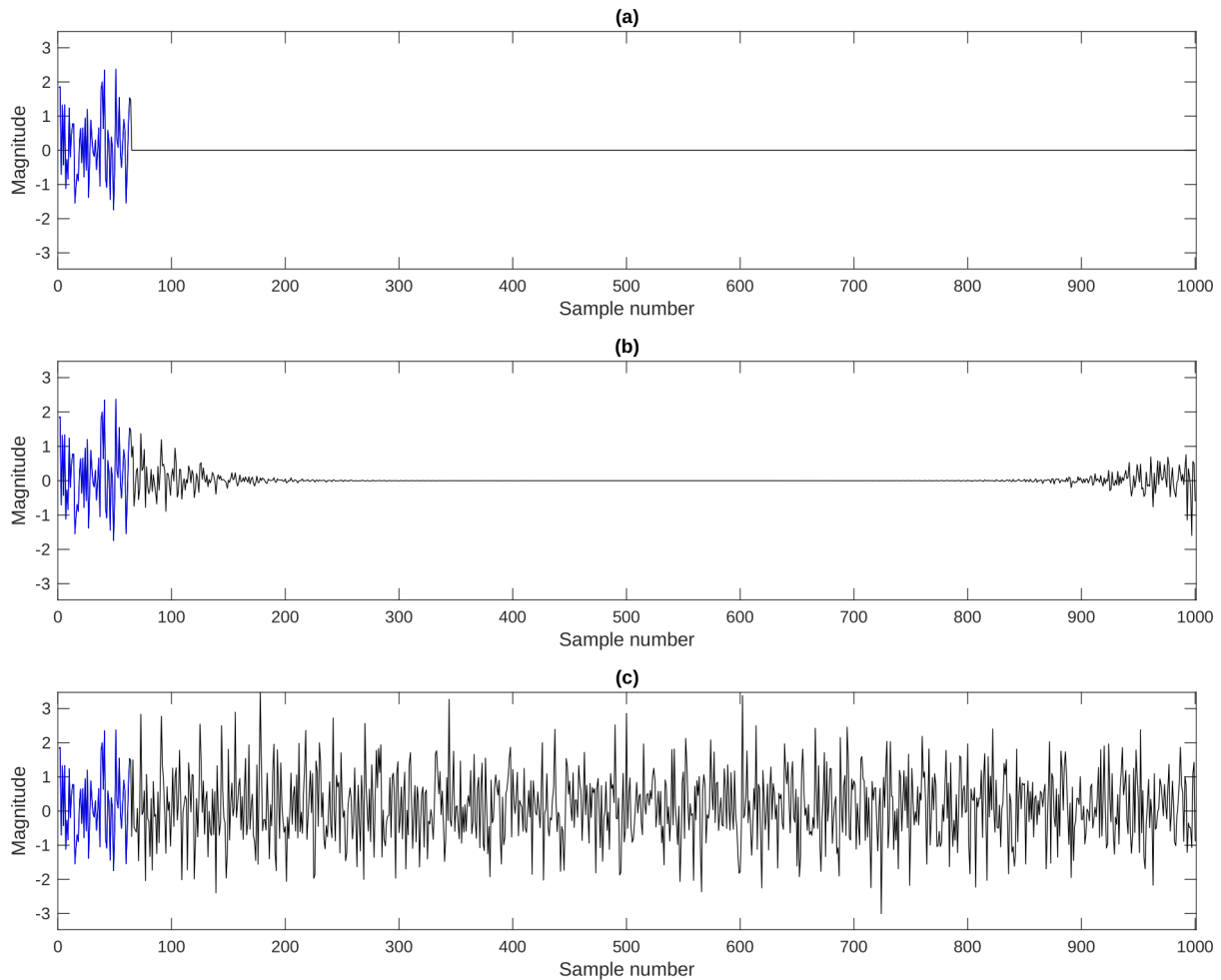


**Figure 9.** White Gaussian noise (blue) and extrapolated data (black) by inverse **(a)** DFT, **(b)** EDFT, **(c)** HRDFT.

## 8 EDFT in MATLAB code

The EDFT package consists of programs written in a simple MATLAB code and is designed to demonstrate the capabilities of EDFT outlined in the previous sections. Each function has a textual help section with comments (%) describing its syntax, algorithm, usage and features. Program EDFT.m and the inverse transform IEDFT.m can be applied to uniform or nonuniform input/output data and frequency sets. From a computational perspective, it makes sense to use the same frequency grid as Fast Fourier Transform (FFT.m in MATLAB library). This allows to apply the FFT algorithm in EDFT calculations, which significantly reduces the computation time, since each FFT requires a number of operations proportional to  $M \log(N)$  instead of  $N^2$  [2]. However, the efficiency of FFT could be between these two values, as it also depends on the value of  $N$ . EDFT.m includes two faster algorithms - with and without NaN (Not a Number) in uniform sequence. The inverse transform to the output of these two algorithms is the MATLAB library program IFFT.m.

**function** [F,S,Stopit]=edft(X,N,I,W,tk)

% EDFT Extended Discrete Fourier Transform.

%

% Function EDFT produce discrete N-point Fourier transform F and amplitude  
% spectrum S of the data vector X. Data X may contain NaN (Not-a-Number).

%

```

% SYNTAX
%
% F=edft(X) or F=edft(X,[]) iteratively computes the Fourier transform of
% data X partially filled with NaN, otherwise Fast Fourier Transform (FFT)
% is applied, F=fft(X).
%
% F=edft(X,N) for length X less than N calculates N-point Fourier transform
% iteratively. If N is vector then EDFT is computed at the query points
% fn defined in N and N set to be equal length(fn). If the length of X
% is greater than N, X is truncated to length N, and EDFT returns the
% same result as fft(X,N) if there is no NaN in X.
%
% F=edft(X,N,I) performs edft(X,N) with limit I to the maximum number of
% iterations. If not specified ([]) , I default to value of parameter
% 'Miteration', edft(X,N)=edft(X,N,Miteration). To complete iteration
% process faster the value for 'Miteration' should be decreased.
%
% F=edft(X,N,I,W) execute edft(X,N,I) with initial conditions defined by
% weight vector W. If not specified ([]) then W=ones(size(F)). W should
% have at least length X nonzero elements for a stable output.
%
% F=edft(X,N,I,W,tk) computes the EDFT of X using the sample points tk.
% If input N is scalar then the EDFT query points calculated as
% fn=(-ceil((N-1)/2):floor((N-1)/2))/N. If tk is not specified ([]) then
% tk=(0:length(X)-1). If the length of tk is greater than X, tk is
% truncated to the length X.
%
% [F,S]=edft(____) returns amplitude spectrum S of data vector X. Vector S
% has the same size and phases as N-point Fourier transform vector F.
% S=F/length(X) in the special case if EDFT output F=fft(X) or F=fft(X,N).
%
% [F,S,Stopit]=edft(____) also returns informative parameter Stopit.
% The first row of Stopit showing the number of performed iteration.
% The second row indicate breaking of iteration reason and may have the
% following values:
% 0 - Maximum number of iteration performed.
% 1 - Sum of outputs division, sum(F./S), is not equal to length(X)*N
% within Relative deviation 'Rdeviat' or no unique solution found. The
% calculations were interrupted because of results may be inaccurate.
% 2 - Relative threshold 'Rthresh' reached. To complete iteration process
% faster the value for 'Rthresh' should be increased.
% The algorithm used by EDFT is output in the third row:
% 0 - A special case where FFT used
% 1 - Faster algorithm for uniform data
% 2 - Algorithm with NaN in uniform data
% 3 - Algorithm for nonuniform data
%
% If X is a matrix, then EDFT treats columns of X as vectors and returns
% the Fourier transform of each column. If N,W,tk are vectors, they are
% applied to each column of X.
%
% ALGORITHM:
%
% Input:
% X - input data.
% N - length of discrete Fourier transform or number of query points in fn.
% I - Algorithms with or without NaN in uniform data number of maximum
% iteration. If not specified, I=Miteration.
% W - weight vector W. If not specified, W = ones(1,N) is used for the
% first iteration.

```

```

% E - Fourier transform basis matrix filled as E=exp(-i*2*pi*tk.*fn).
% The matrix is calculated if algorithm is applied to nonuniform data.
%
% Output F, S for each EDFT iteration is calculated by following formulas:
% R = E*diag(W/N)*E';
% S = (X*inv(R)*E)./diag(E*inv(R)*E).';
% W = S.*conj(S);      W used as input to the next EDFT iteration.
% Algorithms 1 and 2 use functions FFT, IFFT and Levinson-Durbin
% recursion to calculate R faster and speed up matrix multiplication.
%
% A special case:
%     If length of X is equal to N or length fn then EDFT output do not
%     depend on selected weight W and is calculated in non-iterative way.
%
% FEATURES:
%     1. EDFT output F is the N-point Fourier transform of data X. The Power
%     Spectral Density (PSD) function can be calculated by the following
%     formula: abs(F).^2/(N*T), where T is mean sampling period.
%     2. EDFT output S estimate amplitudes and phases of sinusoidal
%     components in the data X.
%     3. EDFT can extrapolate X to the length N. For example, if apply EDFT
%     with N>length(X) get the results: F=edft(X,N)=edft(Y)=fft(Y) and
%     Y=ifft(F), where Y is X plus non-zero forward and backward
%     extrapolation of X to the length N.
%     4. The function IEDFT, call line Y=iedft(F,fn,tn), could be used to
%     calculate the reconstructed sequence Y(tn). If frequencies fn are on
%     the same grid used by FFT algorithm, then MATLAB function ifft can
%     be applied to get uniformly re-sampled and extrapolated to the length(fn)
%     version of input sequence X.
%     5. EDFT can increase frequency resolution N/length(X) times. Division
%     of outputs 1/(T*F./S) demonstrate the frequency resolution of EDFT.
%     The following relationships are true for any EDFT iteration:
%     0<F./S<=N and sum(F./S)=N*length(X).
%     6. EDFT input X may contain NaN which indicate unavailable data or
%     missing samples or data segments.
%
% TIPS for selection of EDFT inputs X(tk) and frequencies fn in N:
%     1. Input sequence X(tk) for EDFT can be sampled uniformly or
%     nonuniformly. Uniform sampling can be considered as a special case of
%     nonuniform sampling, where tk=[0,1,...,K-1]*T. Nonuniform sampling can
%     be realized in many different ways, like as:
%     - uniform sampling with randomly missed samples (known as sparse data);
%     - uniform sampling with missed data segments (known as gapped data);
%     - uniform sampling with jitter: tk=( [0,1,...,K-1] + jitter*rand(1,K) ) * T,
%     where value for jitter is selected in range [0...1];
%     - additive nonuniform sampling: tk=tk-1 + (1+jitter*(rand-0.5)) * T,
%     k=1,...,K-1, t0=0;
%     - signal dependent sampling, e.g., level-crossing sampling, etc.
%     2. Frequencies fn can be selected arbitrary. This mean, that user can
%     choose not only the length of EDFT (number of frequencies in fn) but
%     also the way how to distribute frequencies along the frequency axis.
%     On the other hand, in order to get an adequate representation of X in
%     the frequency domain, fn must cover the entire range in which it is
%     supposed to find components, otherwise EDFT estimate will incorporate
%     power of X components that have spectra outside fn. The analysis of
%     nonuniform X(tk) requires negative and positive frequencies in fn.
%
% See also IEDFT, FFT, IFFT, FFTSHIFT, NUFFT
%
% Author: Vilnis Liepins (vilnisl@gmail.com)

```

```

% References:
% 1) Vilnis Liepins, A spectral estimation method of nonuniformly sampled
% band-limited signals. Automatic Control and Computer Sciences, Vol.28,
% No.2, pp.66-77, 1994.
% 2) Vilnis Liepins, An algorithm for evaluation a discrete Fourier
% transform for incomplete data. Automatic control and computer sciences,
% Vol.30, No.3, pp.27-40, 1996.
% NOTE: The first version of file (gdft.m) was submitted to fileexchange
% on October 7, 1997 as MATLAB 4.1 code.

%=====Set default parameters=====
Miteration=30; % Limit for maximum number of iteration (Stopit 0)
Rdeviat=0.0001; % Value for relative deviation (Stopit 1)
Rthresh=0.0001; % Value for relative threshold (Stopit 2)
%=====Setup input/output arguments=====
if nargin==0||isempty(X), error('Not enough input arguments.').end
% Input argument X
if sum(any(isinf(X))), error('Inf is not allowed in X.').end
if size(X,1)==1, X=X.:',trf=1;else,trf=0;end
[K, L]=size(X);
% Input argument N
fn=[];
if nargin<2||isempty(N)
    N=K;
elseif sum(any(isnan(N)))||sum(any(isinf(N)))
    error('NaN or Inf is not allowed in N.').end
elseif isscalar(N), N=floor(abs(N));% N is a scalar
elseif sum(any(isnan(X)))
    error('NaN is not allowed in X if N is not a scalar.').end
else
    if size(N,1)==1, N=N(:);end % N was vector row
    fn=real(N);[N, NL]=size(fn); % Set frequencies fn
    if NL~=L&&NL~=1, error('Incorrect size of vector N.').end
    elseif NL==1&&L>1,fn=ones(N,L).*fn;end % fn - 2 dim array
    if nargin<5
        tk=ones(K,L).*(0:K-1).'; % Default tk if not specified
        if N<K,tk=tk(1:N,:);end % Truncate tk if more than N points
    end
end
if N<K, X=X(1:N,:);K=N;end % Truncate X if more than N points
% Input argument I
if nargin<3||isempty(I), I=Miteration; % Set default value for I
else
    I=floor(abs(I(1)));
    if isnan(I)||isinf(I), error('NaN and Inf is not allowed in I.').end
end
% Input argument W
if nargin<4||isempty(W), W=ones(N,L); % Set default values for W
elseif sum(any(isnan(W)))||sum(any(isinf(W)))
    error('NaN and Inf is not allowed in W.').end
else
    if size(W,1)==1, W=W(:);end
    [WN, WL] = size(W);
    if WN~=N||(WL~=L&&WL~=1), error('Incorrect size of W.').end
    elseif WL==1&&L>1,W=ones(N,L).*W; % W - 2 dim array
    end
end
W=W.*conj(W);WK=sum(W>0);
for l=1:L
    if WK(l)<K && WK(l)>0, W(:,l)=W(:,l)+max(W(:,l))*Rdeviat;

```

```

elseif WK(1)==0, W(:,1)=ones(N,1);
end
end
% Input argument tk
if nargin==5
if ~isempty(tk)
if sum(any(isnan(X)))||sum(any(isnan(tk)))||sum(any(isinf(tk)))
error('NaN or Inf is not allowed in X and tk.')
```

```

elseif size(tk,1)==1,tk=tk(:);
end
[TK, TL] = size(tk);tk=real(tk);
if TK>K, tk=tk(1:K,:);end % Truncate tk if has more than X points
if TK<K||(TL~=L&&TL~=1), error('Incorrect size of tk.')
```

```

elseif TL==1&&L>1
tk=ones(K,L).*tk; % tk - 2 dim array
end
if isempty(fn)
fn=ones(N,L).*((-ceil((N-1)/2):floor((N-1)/2))/N).';
end
else
tk=ones(K,L).*(0:K-1).'; % Default tk if was empty
end
end
F=zeros(N,L);S=zeros(N,L); % Prefill F and S with zeros
Stopit=[I*ones(1,L);zeros(2,L)];SW=zeros(1,I); % Prefill for Stopit
%=====Process one by one each column of X=====
for l=1:L
Xnan=~isnan(X(:,l)); % Xnan indicate samples as '1' , NaN as '0'
KK=sum(Xnan); % KK the length of input data X w/o NaN
% Check for a special case
if isempty(find(X(:,l),1))||KK==K&&K==N&&isempty(fn)||KK==1&&K==1||KK==0
F(:,l)=fft(X(:,l),N); % Output (F,S) equals to FFT
S(:,l)=F(:,l)/K;
Stopit(:,l)=[1; 0; 0;];
else
% Select an algorithm
if isempty(fn)&&KK==K
Alg=1; % Algorithm without NaN in uniform sequence
elseif KK<K
Alg=2; % Algorithm with NaN in uniform sequence
X(~Xnan,l)=zeros(K-KK,1); % Replace NaN by 0 in X
t=find(Xnan); % Sample number vector
INVR=zeros(K);ER=zeros(K,1);
else
Alg=3; % Algorithm for nonuniform sequence/frequency set
if K==N,I=1;W=ones(N,1);Stopit(:,l)=[1; 0; Alg;];end
E=exp(-1i*2*pi*tk(:,l)*fn(:,l).'); % Complex exponents matrix E
end
XR=zeros(K,1);RE=zeros(K,1);ERE=zeros(N,1);Stopit(3,l)=Alg;
%Start iterations
for it=1:I
if Alg==1
Alg1_ERE;
if stopit1,break,end % Break if Rdeviat reached
F(:,l)=fft(XR,N); % Calculate EDFT output
calc_edft_out;
if stopit2,break,end % Break if Rthresh reached
elseif Alg==2
Alg2_ERE;
if stopit1,break,end % Break if Rdeviat reached
```

```

        F(:,l)=fft(conj(INVR)*X(:,l),N); % Calculate EDFT output
        calc_edft_out;
        if stopit2,break,end % Break if Rthresh reached
    elseif Alg==3
        Alg3_ERE;
        if stopit1,break,end % Break if Rdeviat reached
        F(:,l)=X(:,l).'*RE; % Calculate EDFT output
        calc_edft_out;
        if stopit2,break,end % Break if Rthresh reached
    end
end
end
% End iterations
end
% All columns of X processed
if trf==1,F=F. ';S=S. ';end %Adjust size of EDFT output

%=====Nested functions=====
function st1=stopit1
st1=abs(ERE.*W(:,l)/N/KK-1);st1=false;
if (st1>Rdeviat||isnan(st1))&&(it~=1)
    Stopit(:,l)=[it-1; 1; Alg;];st1=true;
end
end
function st2=stopit2
SW(it)=sum(W(:,l));st2=false;
if it>1
    thit=abs(SW(it-1)-SW(it))/SW(1);
    if thit<=Rthresh
        Stopit(:,l)=[it; 2; Alg;];st2=true;
    end
end
end
function calc_edft_out
S(:,l)=F(:,l)/ERE;
F(:,l)=F(:,l).*W(:,l);
W(:,l)=S(:,l).*conj(S(:,l));
end
function Alg1_ERE
r=ifft(W(:,l));
[a,V]=levinson(r,K-1);
a=a. ';
XR=zeros(K,1);RE=zeros(K,1);rc=a;
for k=1:K/2
    k0=K-k+1;k1=2:K-2*k+1;k2=k+1:K-k;k3=k:K-k+1;
    RE(1)=RE(1)+2*rc(k);
    RE(k0-k+1)=RE(k0-k+1)+2*rc(k0);
    RE(k1)=RE(k1)+4*rc(k2);
    XR(k)=XR(k)+rc(k3)*X(k3,l);
    XR(k0)=XR(k0)+(flipud(rc(k3))).*X(k3,l);
    XR(k2)=XR(k2)+rc(k2)*X(k,l)+flipud(conj(rc(k2))).*X(k0,l);
    rc(k2)=rc(k2-1)+conj(a(k+1))*a(k2)-a(k0)*flipud(conj(a(k2+1)));
end
if mod(K,2)==1
    RE(1)=RE(1)+rc(k+1);XR(k+1)=XR(k+1)+X(k+1,l)*rc(k+1);
end
ERE=real(fft(RE,N));W(:,l)=W(:,l)/real(V);
end
function Alg2_ERE
R=Alg2_R;

```

```

if rcond(R(t,t))>eps
    INVR(t,t)=R(t,t)\eye(KK);
else
    W(:,1)=W(:,1)+Rdeviat*max(W(:,1));
    R=Alg2_R;
    INVR(t,t)=pinv(R(t,t));
end
ER(1)=trace(INVR);
for k=1:K-1
    ER(k+1,1)=sum(diag(INVR,k)+conj(diag(INVR,-k)));
end
ERE=real(fft(ER,N));
function R=Alg2_R
    RT=ifft(W(:,1));
    R=toeplitz(RT(1:K));
end
end
function Alg3_ERE
    R=Alg3_R;
    if rcond(R)>eps
        RE=R\E;
    else
        W(:,1)=W(:,1)+Rdeviat*max(W(:,1));
        R=Alg3_R;
        RE=pinv(R)*E;
    end
    ERE=sum(conj(E).*RE).';
    function R=Alg3_R
        R=E*diag(W(:,1)/N)*E';
    end
end
end
end

function [Y,t]=iedft(F,fn,tn)

%IEDFT Inverse Extended Discrete Fourier Transform.
%
% Y=iedft(F,fn,tn) is the inverse Fourier transform of EDFT output F
% (see help edft) evaluated at the query points fn, where sample points
% tn of Y can be uniform or non-uniform.
%
% [Y,t]=iedft(____) returns also sample points t of output Y.
%
% If fn is not specified ([]) then IEDFT is calculated at the query points
% fn=(-ceil((N-1)/2):floor((N-1)/2))/N, where N=length(F).
%
% If tn is not specified ([]) then IEDFT use uniform time points tn=0:N-1.
%
% In the special case of uniform fn and tn, IEDFT can be replaced by
% well-known MATLAB IFFT function.
%
% If F is a matrix, then IEDFT treats columns of F as vectors and returns
% the inverse Fourier transform of each column. If fn,tn are vectors,
% they are applied to each column of F.
%
% See also EDFT, IFFT, FFT
%
% Author: Vilnis Liepins (vilnisl@gmail.com)

% Check input argument F

```

```

if nargin<1,error('Not enough input arguments.')
```

```
elseif sum(any(isnan(F)))||sum(any(isinf(F)))
```

```
    error('NaN and Inf is not allowed in F.')
```

```
end
```

```
if size(F,1)==1
```

```
    trf=1;
```

```
    F=F.:';
```

```
else
```

```
    trf=0;
```

```
end
```

```
[N,L]=size(F);
```

```
% Check input argument fn
```

```
if nargin<2||isempty(fn)
```

```
    fn=ones(N,L).*((-ceil((N-1)/2):floor((N-1)/2))/N).';
```

```
elseif sum(any(isnan(fn)))||sum(any(isinf(fn)))
```

```
    error('NaN or Inf is not allowed in fn.')
```

```
else
```

```
    if size(fn,1)==1,fn=fn(:);end    % fn was vector row
```

```
    fn=real(fn);
```

```
    if size(fn,1)~=N,error('Incorrect size of fn. '),end
```

```
    if size(fn,2)==1&&L>1,fn=ones(N,L).*fn;end % fn is 2 dim array
```

```
    if size(fn,2)~=L,error('Incorrect size of fn. '),end
```

```
end
```

```
% Check input argument tn
```

```
if nargin<3||isempty(tn)
```

```
    tn=ones(N,L).*(0:N-1).';
```

```
elseif sum(any(isnan(tn)))||sum(any(isinf(tn)))
```

```
    error('NaN or Inf is not allowed in tn.')
```

```
else
```

```
    if size(tn,1)==1, tn=tn(:);end    % tn was vector row
```

```
    tn=real(tn);[TR,TC]=size(tn);
```

```
    if TC~=L&&TC~=1,error('Incorrect size of tn. '),end
```

```
    if TC==1&&L>1,tn=ones(TR,L).*tn;end % tn is 2 dim array
```

```
end
```

```
% Set default values for Y
```

```
Y=zeros(size(tn));
```

```
% Calculate IEDFT for each F column l
```

```
for l=1:L
```

```
    E=exp(1i*2*pi*tn(:,l)*fn(:,l).');
```

```
    Y(:,l)=E*F(:,l)/N;
```

```
end
```

```
% Adjust size of output
```

```
if trf==1,Y=Y.:';t=tn.:'; else,t=tn;end
```

The next program demonstrates the applicability of the Extended DFT in 2-dimensional signal processing. The EDFT2.m program is based on the MATLAB library program FFT2.m where FFT.m calls are replaced by EDFT.m. The inverse transform to EDFT2.m is the MATLAB library program IFFT2.m.

**function f = edft2(x,mrows,ncols)**

```

% EDFT2 Two-dimensional Extended Discrete Fourier Transform.
%
%     EDFT2(X) returns the two-dimensional Fourier transform of matrix X.
%     Before run EDFT2 unknown data (if any) inside of X should be replaced
%     by NaN (Not-a-Number).
%     If X is a vector, the result will have the same orientation.
%     EDFT2(X,MROWS,NCOLS) performing size MROWS-by-NCOLS Fourier transform
%     without padding of matrix X with zeros.
```

```

%
% See also EDFT, FFT2, IFFT2.
%
% EDFT2 is created on basis of FFT2 (J.N. Little 12/18/1985) by Vilnis Liepins.

% No input
if nargin==0, error('Not enough input arguments. '),end
if sum(any(isinf(x))), error('Inf is not allowed in input. '),end
[m, n] = size(x);
% Basic algorithm
if (nargin == 1) && (m > 1) && (n > 1)
% f = fft(fft(x).').';
f = edft(edft(x).').';
return;
end
% Padding for vector input
if nargin < 3, ncols = n; end
if nargin < 2, mrows = m; end
mpad = mrows; npad = ncols;
if m == 1 && mpad > m, x(2, 1) = 0; m = 2; end
if n == 1 && npad > n, x(1, 2) = 0; n = 2; end
if m == 1, mpad = npad; npad = 1; end % For row vector
% Preprocessing
if n > 1, x = ifft(edft(x.', npad)).'; end
% Transform
%f = fft(x, mpad);
f = edft(x, mpad);
if m > 1 && n > 1, f = fft(f.', npad).'; end

```

The first version of EDFT (file GDFT.m) was submitted to file-exchange server on 10/7/1997 as MATLAB 4.1 code. The renewed code version uploaded on 8/5/2006 and available online [mathworks.com](http://mathworks.com) and [researchgate.net](http://researchgate.net).

Run MATLAB program EDFT\_FIG.m available on [mathworks.com](http://mathworks.com) to recreate all the computer simulations presented in this article.

## 9 References

- [1] D. Slepian, H.O. Pollak. Prolate Spheroidal Wave Functions, Fourier Analysis and Uncertainty - I. Bell System Technical Journal, Vol.40 No.1, pp.43-63, 1961.
- [2] James W. Cooley, John W. Tukey. An algorithm for the machine calculation of complex Fourier series. Math. Comput., Vol.19, pp.297-301, 1965.
- [3] S.M. Kay, S.L. Marple. Spectrum analysis - a modern perspective. Proc. IEEE, Vol.69, No.11, 1981.
- [4] Vilnis Liepins. A method for spectral analysis of band-limited signals, Automatic Control and Computer Sciences. Vol.27, No.5, pp.56-63, 1993. Available on [researchgate.net](http://researchgate.net).
- [5] Vilnis Liepins. A method of spectrum evaluation applicable to analysis of periodically and non-regularly digitized signals. Automatic Control and Computer Sciences, Vol.27, No.6, pp.57-64, 1993. Available on [researchgate.net](http://researchgate.net).
- [6] Vilnis Liepins. A spectral estimation method of nonuniformly sampled band-limited signals. Automatic Control and Computer Sciences, Vol.28, No.2, pp.66-73, 1994. Available on [researchgate.net](http://researchgate.net).
- [7] Vilnis Liepins. An algorithm for evaluation a discrete Fourier transform for incomplete data. Automatic Control and Computer Sciences, Vol.30, No.3, pp.27-40, 1996. Available on [researchgate.net](http://researchgate.net).

[8] Vilnis Liepins. High-resolution spectral analysis by using basis function adaptation approach. Doctoral Thesis for Scientific Degree of Dr.Sc.Comp. /in Latvian/, University of Latvia, 1997. Available on [researchgate.net](http://researchgate.net).

[9] M.D. Sacchi, T.J. Ulrych, C. Walker. Interpolation and extrapolation using a high-resolution discrete Fourier transform. IEEE Trans. on Signal Processing, Vol.46, No.1, pp.31-38, 1998.

Many thanks to all authors of articles [10-54] for using EDFT approach in their research and applications!

## 10 Related articles

[10] Modris Greitans. Multiband signal processing by using nonuniform sampling and iterative updating of autocorrelation matrix. Proceedings of the 2001 International Conference on Sampling Theory and Application, May 13-17, 2001, Orlando, Florida, USA, pp.85-89.

[11] Modris Greitans. Spectral analysis based on signal dependent transformation. The 2005 International Workshop on Spectral Methods and Multirate Signal Processing, (SMMSP 2005), June 20-22, 2005, Riga, Latvia.

[12] Jayme Garcia Arnal Barbedo, Amauri Lopes, Patrick J. Wolfe. High Time-Resolution Estimation of Multiple Fundamental Frequencies. Proceedings of the 8th International Conference on Music Information Retrieval, ISMIR 2007, September 23-27, Vienna, Austria, pp.399-402.

[13] David Dolenc, Barbara Romanowicz, Paul McGill, William Wilcock. Observations of infragravity waves at the ocean-bottom broadband seismic stations Endeavour (KEBB) and Explorer (KXBB). Geochemistry, Geophysics, Geosystems, Vol.9, Issue 5, May 2008.

[14] Quanming Zhang, Huijin Liu, Hongkun Chen, Qionglin Li, Zhenhuan Zhang. A Precise and Adaptive Algorithm for Interharmonics Measurement Based on Iterative DFT. IEEE Trans on Power Delivery, Vol.23, Issue 4, pp.1728-1735, October 2008.

[15] Petre Stoica, Jian Li, Hao He. Spectral Analysis of nonuniformly Sampled Data: A New Approach Versus the Periodogram. IEEE Trans on Signal Processing, Vol.57, Issue 3, pp.843-858, March 2009.

[16] Eric Greenwood, Fredric H. Schmitz. Separation of Main and Tail Rotor Noise Sources from Ground-Based Acoustic Measurements Using Time-Domain De-Dopplerization. 35th European Rotorcraft Forum 2009, September 22-25, Hamburg, Germany.

[17] Jayme Garcia Arnal Barbedo, Amauri Lopes, Patrick J. Wolfe. Empirical Methods to Determine the Number of Sources in Single-Channel Musical Signals. IEEE Transactions on Audio, Speech and Language Processing, Vol.17, Issue 7, pp.1435-1444, September 2009.

[18] Tarik Yardibi, Jean Li, Petre Stoica, Ming Xue, Arthur B. Baggeroer. Source localization and sensing: A nonparametric iterative adaptive approach based on weighted least squares. IEEE Transactions on Aerospace and Electronic Systems, Vol.46, pp.425-443, January 2010.

[19] M. Caciotta, S. Giarnetti, F. Leccese, Z. Leonowicz. Comparison between DFT, adaptive window DFT and EDFT for power quality frequency spectrum analysis. Modern Electric Power Systems (MEPS), 2010 Proceedings of the International Symposium, Sept.20-22, 2010, Wroclaw, pp.1-5.

[20] Li, Yan Zheng, Wang Xing-zhi. Inter-harmonic Analysis Using IGG and Extended Fourier. Proceedings of the Chinese Society of Universities for Electric Power System and its Automation, 22(3), 2010.

[21] Erik Gudmundson, Andreas Jakobsson, Jörgen Jensen, Peter Stoica. An Iterative Adaptive Approach for Blood Velocity Estimation Using Ultrasound. EUSIPCO 2010, August 23-27, Aalborg, Denmark, pp.348-352.

- [22] Modris Greitans, Rolands Shavelis. Reconstruction of sequences of arbitrary shaped pulses from its low pass or band pass approximations using spectrum extrapolation. EUSIPCO 2010, August 23-27, Aalborg, Denmark, pp.1607-1611.
- [23] Juggrapong Treetrong. Fault Detection of Electric Motors Based on Frequency and Time-Frequency Analysis using Extended DFT. International Journal of Control and Automation, Vol.4, No.1, March 2011.
- [24] Jesper Rindom Jensen, Mads Græsbøll Christensen, Søren Holdt Jensen. A Single Snapshot Optimal Filtering Method for Fundamental Frequency Estimation. 36th International Conference on Acoustics, Speech and Signal Processing (ICASSP), Prague, Czech Republic, May 22-27, 2011, pp. 4272-4275.
- [25] Ming Xue, Luzhou Xu, Jian Li. IAA spectral estimation: fast implementation using the Gohberg-Semencul factorization. ICASSP 2011, May 22-27, Prague, Czech Republic, pp.3251-3261.
- [26] Bonifatius Wilhelmus Tilma. Supervisor: M.K. Smit; Co-promotor: E.A.J.M. Bente. Integrated tunable quantum-dot laser for optical coherence tomography in the 1.7 $\mu$ m wavelength region. Eindhoven, Technische Universiteit Eindhoven, Diss., January 2011.
- [27] Elmar Mair, Michael Fleps, Michael Suppa, and Darius Burschka. Spatio-temporal initialization for IMU to camera registration. In Proceedings of the IEEE International Conference on Robotics and Biomimetics (ROBIO), December 2011, pp.557-564.
- [28] George-Othan Glentis, Andreas Jakobsson. Superfast Approximative Implementation of the IAA Spectral Estimate. IEEE Transactions on Signal Processing, Vol.60, Issue 1, January 2012, pp.472-478.
- [29] B. W. Tilma, Yuqing Jiao, J. Kotani, B. Smalbrugge, H. P. M. M. Ambrosius, P. J. Thijs, X. J. M. Leijtens, R. Notzel, M. K. Smit, E. A. J. M. Bente. Integrated Tunable Quantum-Dot Laser for Optical Coherence Tomography in the 1.7  $\mu$ m Wavelength Region. IEEE Journal of Quantum Electronics, Vol.48, No.2, February 2012, pp. 87-98.
- [30] T. Odstrcil, M. Odstrcil, O. Grover, V. Svoboda, I. Ďuran, and J. Mlynář. Low cost alternative of high speed visible light camera for tokamak experiments. Review of Scientific Instruments. Oct.2012, Vol.83, Issue 10.
- [31] Elmar Mair. Co-promotor: Gregory Donald Hager. Efficient and Robust Pose Estimation Based on Inertial and Visual Sensing. München, Technische Universität München, Diss., 2012.
- [32] Akash K Singh. Quantum-Dot Laser OCT. International Journal of Engineering Research and Applications (IJERA), Vol.2, Issue 6, November – December 2012, pp.340-371.
- [33] Elliot Briggs, OFDM Physical Layer Architecture and Real-Time Multi-Path Fading Channel Emulation for the 3GPP Long Term Evolution Downlink. PhD Thesis. Texas Tech University, December 2012.
- [34] Kwadwo S. Agyepong. Fang-Han Hsu, Edward R. Dougherty and Erchin Serpedin. Spectral Analysis on Time-Course Expression Data: Detecting Periodic Genes Using a Real-Valued Iterative Adaptive Approach. Advances in Bioinformatics, Vol.2013.
- [35] Matthew James Kelley. Terahertz time domain spectroscopy of amino acids and sugars. Dissertation (Ph.D.), California Institute of Technology, March 2013.
- [36] Vsevolod Kharyton, Ronnie Bladh. Using Tiptiming and Strain Gauge Data for the Estimation of Consumed Life in a Compressor Blisk Subjected to Stall-Induced Loading. ASME Turbo Expo 2014: Turbine Technical Conference and Exposition, Vol.7B, June 16–20, 2014, Düsseldorf, Germany.
- [37] Hui Wang, Cancan Liu, Bing Zhu, Juanjuan Cai & Yutian Wang. Multi-pitch estimation based on correlation and spectrum analysis. ICCT, Future Communication Technology, 2014.
- [38] D. Krause, W. B. Hussein, M. A. Hussein, T. Becker. Ultrasonic sensor for predicting sugar concentration using multivariate calibration. Ultrasonics, 54(6), 1703-1712, August 2014.

- [39] Petre Stoica, Dave Zachariah, Jian Li. Weighted SPICE: A Unifying Approach for Hyperparameter-Free Sparse Estimation, *Digital Signal Processing*, Vol.33, pp.1-12, October 2014.
- [40] D.T. Michel, A.K. Davis, W. Armstrong, R. Bahr, R. Epstein, V.N. Goncharov, M. Hohenberger, I.V. Igumenshchev, R. Jungquist, D.D. Meyerhofer, P.B. Radha, T.C. Sangster, C. Sorce and D.H. Froula. Measurements of the ablation front trajectory and low-mode nonuniformity in direct-drive implosions using x-ray self-emission shadowgraphy. *High Power Laser Science and Engineering*, Vol.3, E19, July 2015.
- [41] Jan Kober, Zdenek Prevorovsky, Milan Chlada. In situ calibration of acoustic emission transducers by time reversal method. *Sensors and Actuators A: Physical*, Vol.240, pp.50–56, April 2016.
- [42] Stephanie Tsuei, Mark B. Milam. Trajectory generation for constrained differentially flat systems with time and frequency domain objectives. *IEEE 55th Conference on Decision and Control (CDC)*, pp.4172-4177, December 2016.
- [43] L.Luzi, A.Stevens, H.Yang, M.D.Browning. Resolution Versus Error for Computational Electron Microscopy. *Microscopy and Microanalysis*, 23(S1), pp.88-89, August 2017.
- [44] Stavroula Karatasou and Mat Santamouris, Multifractal Analysis of High-Frequency Temperature Time Series in the Urban Environment, *Climate* 2018, 6(2), 50.
- [45] L.Jinxiang, J.Lin, L.Weidong, D.Jiejie. Interharmonic Detection Based on Iterative Spectrum Estimation and SVM. *2018 China International Conference on Electricity Distribution (CICED)*. IEEE, pp.867-871, September 2018.
- [46] Seyed Abdolmajid Yousefsani, Hooman Dejnabadi, Olivier Guyen, Kamiar Aminian. A Vibrational Technique for in vitro Intraoperative Prosthesis Fixation Monitoring. *IEEE Transactions on Biomedical Engineering*, Vol.67, No.10, October 2020.
- [47] Maxime Schutz, Cyril Decroze, Michele Lalande, Bertrand Lenoir. Neural Networks to Increase Range Resolution of FMCW Radar. *IEEE Sensors Letters*, Volume 4, Issue 8, August 2020.
- [48] Valeria Mundaca-Moraga, Rodrigo Abarca-del-Rio, Dante Figueroa, James. A Morales. Preliminary Study of Wave Energy Resource Using an HF Marine Radar, Application to an Eastern Southern Pacific Location: Advantages and Opportunities. *Remote Sensing*, Volume 13, Issue 2, 2021.
- [49] Zhipeng Lin, Tiejun Lv, Wei Ni, J. Andrew Zhang, Jie Zeng, Ren Ping Liu. Joint Estimation of Multipath Angles and Delays for Millimeter-Wave Cylindrical Arrays with Hybrid Front-ends. *IEEE Transactions on Wireless Communications*, Volume 20, Issue 7, 2021.
- [50] Lei Zhang, Qizhi Zhao, Cheng Fan. Dwell time algorithm in deterministic polishing of a free-form surface based on the continuous tool influence function. *Appl. Opt.*, Volume 60, Issue 9, March 2021.
- [51] G. Nachmani, T. Mazeh, and N. Sochen. COD: An algorithm for shape reconstruction of transiting celestial bodies through topological optimization. *Monthly Notices of the Royal Astronomical Society*, January 2022.
- [52] Yonas Lebsir, Sergejs Boroviks, Martin Thomaschewski, Sergey I. Bozhevolnyi, Vladimir A. Zenin. Ultimate limit for optical losses in gold, revealed by quantitative near-field microscopy, arXiv:2203.00754 [physics.optics], March 2022.
- [53] Chenxu Zhang, Short-term electricity price point and probabilistic forecasts. *Theses and Dissertations*, Mississippi State University, August 2022.
- [54] Ji-Wang ZHANG, Xu ZHANG, Ke-Qin DING, Rong-Ren WANG and Ya-Nan HU. Parameter Identification Method of Nonuniform and Under-Sampled Blade Tip Timing Based on Extended DFT and Compression Sensing. Oct 2022, available at SSRN: <https://ssrn.com/abstract=4239336>.